Ceramic Turbine Components Research and Development

Part 2: Evaluation of MCrAlY/ZrO_2 (Y_2O_3) Thermal-Barrier Coatings Exposed to Simulated Gas Turbine Environments

---

AP-1539, Part 2
Research Project 421-1

Final Report, August 1980

Prepared by

WESTINGHOUSE ELECTRIC CORPORATION
Research and Development Center
1310 Beulah Road
Pittsburgh, Pennsylvania 15235

Principal Investigators
S. C. Singhal
S. Y. Lee

Program Manager
R. J. Bratton

Prepared for

Electric Power Research Institute
3412 Hillview Avenue
Palo Alto, California 94304

EPRI Project Manager
A. Cohn

Power Generation Program
Advanced Power Systems Division

ORDERING INFORMATION

Requests for copies of this report should be directed to Research Reports Center (RRC), Box 50490, Palo Alto, CA 94303, (415) 965-4081. There is no charge for reports requested by EPRI member utilities and affiliates, contributing nonmembers, U.S. utility associations, U.S. government agencies (federal, state, and local), media, and foreign organizations with which EPRI has an information exchange agreement. On request, RRC will send a catalog of EPRI reports.

NOTICE

This report was prepared by the organization(s) named below as an account of work sponsored by the Electric Power Research Institute, Inc. (EPRI). Neither EPRI, members of EPRI, the organization(s) named below, nor any person acting on their behalf: (a) makes any warranty or representation, express or implied, with respect to the accuracy, completeness, or usefulness of the information contained in this report, or that the use of any information, apparatus, method, or process disclosed in this report may not infringe privately owned rights; or (b) assumes any liabilities with respect to the use of, or for damages resulting from the use of, any information, apparatus, method, or process disclosed in this report.

Prepared by
Westinghouse Electric Corporation
Pittsburgh, Pennsylvania

ABSTRACT

The purpose of this study was to determine the resistance of two state-of-the-art duplex thermal barrier coating systems to utility turbine combustion gases. These coating systems are of interest because large electricity cost savings could be achieved if the coatings permit turbine operation with residual fuels at distillate-rated firing temperatures, and substantial savings in fuel and capital cost may be achieved through increased turbine inlet temperature. The coating systems evaluated consisted of a MCrAlY (M = Ni or Ni/Co) bond coat and ZrO_2 stabilized with 12 wt% Y_2O_3 overcoat, each deposited by plasma arc spray on Udimet-500 turbine alloy specimens. The corrosion testing was conducted in a pressurized turbine test passage at 2000°F gas temperature using GT-2 diesel oil and that containing Na, V, P and S contaminants. Post-test analysis showed that the coatings performed well when exposed to clean GT-2 fuel and that containing 1 ppm Na or 5 ppm Pb; but in the presence of vanadium and/or phosphorous in the fuel, the ZrO_2 - 12 wt% Y_2O_3 coating deteriorated through severe cracking and eventual spalling. Various possible causes for the oxide coating degradation are discussed. This work shows that the thermal barrier coating concept is feasible for utility turbines, but coating development specifically for utility turbines burning residual fuels will be required.

EPRI PERSPECTIVE

PROJECT DESCRIPTION

This project was planned to coordinate with the Department of Defense-Advanced Research Projects Agency (DARPA) program on the application of ceramics to combustion turbines. That program was developing ceramic first-stage turbine stator vanes and a special gas turbine to test the vanes to elevated turbine inlet temperatures. Analysis showed that there was a much greater power and efficiency advantage when the ceramic's high-temperature capability could be applied to the rotor blade as well as the first stator vane. RP421 was planned to design and fabricate the ceramic rotor blades to run in the special DARPA engine. During the first year of this project the DARPA program was curtailed and the special engine canceled. The RP421 blade-fabrication task was canceled, and work concentrated on an investigation of the ceramic blade-metal rotor interface engineering, which had surfaced as a key technical barrier in doing the ceramic blade design. The ceramic-metal interface problem was extended to include ceramic coatings of metal blades and vanes for use as thermal barriers and corrosion protectors and to ceramic combustor elements for use as supports for catalytic combustion inside metal combustor cans. Previous work, done by NASA, on ceramic thermal-barrier coatings had shown promising durability in the combustion products of clean, light aviation-type fuels. The durability of the coatings has not been investigated using heavy oil-type fuels. Catalytic combustors had previously demonstrated very low emissions in laboratory-type test setups. The mechanical integration of the catalytic elements into the industrial gas turbine engine had not previously been engineered.

PROJECT OBJECTIVE

The project's objective was to investigate the problem areas of utilizing ceramic components in combustion turbines. The ceramic components included monolithic ceramic turbine blades attached to the metal rotor, ceramic coatings of metal turbine vanes and blades as a thermal barrier, and ceramic substrates for catalyst supports in catalytic combustors. This investigation was to determine the most promising applications of ceramics and to plan the projects needed to develop these to practicality.

PROJECT RESULTS

1. Ceramic Rotor-Blade Development

While advances were made in blade-root design, the use of compliant layers, and intermediate piece attachment, it is considered that monolythic ceramic blades and vanes are not yet ready to be developed for incorporation into utility-scale combustion turbines. There is first required the preliminary development of (1) improved materials with higher temperature and better corrosion-erosion resistance capability, (2) better and more consistent fabrication techniques, (3) improved failure criteria and prediction techniques, and (4) greatly improved nondestructive evaluation methods to separate the flawed from the acceptable components. These problem areas are currently being investigated by DARPA and the Navy in a project for a 1000-hp ship engine. The utility industry should first wait until such projects have (hopefully) successfully demonstrated the capability of smaller ceramic-bladed turbines before considering applying the technology to utility-scale machines.

2. Ceramic Thermal-Barrier Coatings

This project had the first tests in which ceramic thermal-barrier coatings were subject to combustion gases containing the impurities often found in utility fuel. The coating types, which had performed successfully in previous clean fuel tests, were found to spall badly when the fuel contained vanadium, even when a magnesium inhibitor was added. As a result of this project, RP1039 with NASA (for the purpose of developing thermal-barrier blade coatings), was restructured to concentrate on determining the compatibility of various coatings with fuel impurities.

3. Ceramic Catalytic Combustor Design

This project established a reference design for the catalytic combustor. The thermal and mechanical analyses of the catalytic ceramic element and the supporting metal structures showed them capable of operating over the whole range of combustion-turbine operation. Experimentally measured temperature profiles determined the range of flow velocity and burner-inlet temperature required for good catalyst operation. These measurements also showed the large effect that precombustion ahead of the catalyst had on elevating catalyst efficiency. A plan for

developing reliable catalytic combustors was formulated. This plan forms a basis for RP1657 that will develop the reliable utility-scale catalytic combustor.

A. Cohn, Project Manager
Advanced Power Systems Division

ACKNOWLEDGMENTS

The authors acknowledge invaluable contributions of the following personnel in the performance of this investigation:

- S. R. Levine, NASA-Lewis Research Center, for supplying part of the coatings and helpful discussions.
- C. J. Spengler for exposing uncooled coated solid specimens in his on-going tests in the pressurized turbine passage.
- R. C. Kuznicki and T. A. Manion for X-ray diffraction analyses.
- R. W. Palmquist and J. J. Haugh for electron microprobe analyses.
- J. Valentich for thermal expansion measurements.
- G. A. Blann for metallographic photography.
- J. A. Fraino for excellent technical assistance.

CONTENTS

ILLUSTRATIONS

TABLES

SUMMARY

The thermal barrier coating concept for gas turbines is to provide an insulating protective layer between the hot gas and critical air-cooled metal components. If successfully applied, the concept will allow near term engine design tradeoffs with sizeable economic benefits. Turbine inlet temperature, e.g., may be increased to improve thermodynamic efficiency while maintaining the same coolant flow schedule and hence metal temperature without sacrificing component life. Or current turbine inlet temperatures could be maintained and efficiency increases gained by reducing air flow schedule to maintain the same metal temperature without sacrificing component life. Similarly, component life could be greatly extended by maintaining current gas temperatures and coolant flow and reducing metal temperatures.

The potential benefits of ceramic thermal barrier coatings on large power generation gas turbines have been determined by Westinghouse and United Technologies through a NASA-sponsored program (1-3). These studies showed large electricity cost savings especially if the coatings permit turbine operation with residual fuels at distillate-rated firing temperatures. The increased turbine firing temperatures possible with the coatings also resulted in substantial cost savings.

In order to be successful, the thermal barrier coatings must withstand the thermal/mechanical loads imposed by temperature gradients and thermal cycling without spalling—the actual breaking away of the coating from the metal surface. The coating must also be structurally stable in the combustion environment of utility gas turbines.

NASA-Lewis demonstrated through rig and engine testing that a simple, two-layer plasma-sprayed thermal barrier coating system has the potential for protecting high temperature air-cooled combustion turbine components (4). Of the initially examined coatings, the most promising system for aircraft gas turbines was a Ni-16Cr-6Al-.6Y bond coating (~5 mil thick) and a ZrO_2-12 wt% Y_2O_3 thermal barrier coating. This coating was found as predicted to substantially lower the metal

temperature of the air-cooled airfoils tested (280° to 375°F). In burner rigs the coating withstood 3200 cycles of cooling from a 2340°F surface temperature and 275 cycles of cooling from 2714°F without cracking or spalling. In engine testing the coating successfully withstood 35 start-stop thermal cycles with a total testing time of 150 hours at turbine inlet temperatures as high as 2500°F and 500 2-minute cycles from 2500°F to flame-out with no signs of deterioration. However, preliminary hot corrosion tests with sea salt injected into the flame at gas temperatures of 1650°F indicated coating adherence problems after 40 1-hour cycles (5).

The purpose of this EPRI Program (RP 421-1) was to determine the behavior of the NASA-type duplex thermal barrier coatings in present and anticipated environments of utility gas turbines. The results of the program, although preliminary, provide a basis for planning the future work needed to use thermal barrier coatings in utility systems.

The corrosion evaluation of two duplex thermal barrier coating systems, consisting of MCrAlY (M = Ni or Ni/Co) bond coat and ZrO_2-12 wt% Y_2O_3 ceramic overcoat was conducted in a pressurized test passage at 2000°F gas temperature. The main test specimens were instrumented air-cooled cylinders of Udimet-500 alloy to which the bond coat and ceramic coatings were applied by plasma arc spray. The coatings were deposited both by NASA-Lewis and the Linde Div. The combustion atmospheres were varied by doping clean GT-2 fuel with the desired concentrations of sodium, sulfur and vanadium. Fuel additives commonly used to prevent corrosion attack of metals were also employed when residual fuels were simulated.

Initial coating evaluations were made using rather complex combustion atmospheres distributed by on-going tests at Westinghouse. A final evaluation was based on a systematic study of the effects of individual fuel contaminants on the corrosion behavior of the coatings.

The results of this program clearly showed that the NASA-type coatings performed well when exposed to clean GT-2 fuel and even that containing either 1 ppm Na or 5 ppm Pb; but in the presence of vanadium and/or phosphorous (a tramp impurity) in the fuel, the ZrO_2-12 wt% Y_2O_3 coating deteriorated through severe cracking and eventual spalling within about 40 hours of exposure. A high reactivity of the Y_2O_3 in the ZrO_2-12 wt% Y_2O_3 coating toward vanadium and phosphorous, which caused destabilization of the zirconia coating as well as the formation of new compounds, was identified as the principal failure modes. These and other possible contributing

factors reflect the fact that the state-of-the-art coatings are not optimized for utility turbines burning residual fuels. Several approaches to minimize reaction problems with vanadium containing fuels have been identified.

The principal conclusions from this study are: 1) the thermal barrier coating concept is feasible for utility turbines, but 2) improved and/or new coating compositions will need to be developed specifically for utility turbines burning residual fuels.

REFERENCES

1. D. J. Amos. Analytical Investigations of Thermal Barrier Coatings on Advanced Power Generation Gas Turbines. NASA CR-135146, March 1977.

2. N. Carlson and B. L. Stone. Thermal Barrier Coatings on High Temperature Gas Turbine Engines. NASA CR-135147, February 1977.

3. J. S. Clark, J. J. Nainiger and R. E. Heyland. Potential Benefit of a Ceramic Thermal Barrier Coating on Large Power Generation Gas Turbines. NASA TM 73712, June 1977.

4. S. Stecura. Two-Layer Thermal Barrier Coating for High Temperature Components. Bull. Am. Ceram. Soc. 56 (12) 1977.

5. S. R. Levine and J. S. Clark. Thermal Barrier Coatings--A Near Term High Payoff Technology. NASA TM X-73586, 1977.

Section 1

INTRODUCTION

There is considerable incentive to increase gas inlet temperature in power generation gas turbines to improve thermal efficiency and increase power output for a given engine size. Because of the difficulty in achieving major improvements in temperature capabilities of metallic alloy systems and the significant losses in turbine efficiency in using airfoil cooling, serious consideration is being given to coating the metal components with a thermally insulating ceramic material for maintaining metal components at much lower temperatures than the hot combustion gases (1-6). Potential benefits from the use of such thermal barrier coatings are quite large and include reduction of metal temperature by about 200°-400°F or reduction in cooling air requirements. Studies conducted by United Technologies (7) and Westinghouse (8) have shown that thermal barrier coatings provide an attractive potential means to improve performance and reductions in cost of electricity, the greatest savings in cost of electricity occurring in the case of utility turbine operation on residual fuels at distillate rated firing temperatures. Moreover, significant performance improvements and reductions in cost of electricity can be achieved in very near term by increasing the turbine inlet temperature in today's combined cycle power plants. Thus, these thermal barrier coatings may well provide the transition between metallic systems and the apparent ultimate solution of bulk ceramic airfoils.

A two-layer thermal barrier coating consisting of yttria-stabilized zirconia over a NiCrAlY bond coat, shown schematically in Figure 1-1, has recently been investigated at the NASA-Lewis Research Center (1-6). Their research program identified yttria-stabilized zirconia as being superior to other coating compositions on the basis of adherence to the NiCrAlY bond coat, thermal shock resistance, and resistance to cracking. The tests in an operating type gas turbine engine showed that the NiCrAlY/$ZrO_2(Y_2O_3)$ coating successfully withstood 35 start-stop thermal cycles (total testing time of 150 h) at turbine inlet temperatures as high as 2500°F and 500 2-min cycles from 2500°F to flame-out with no signs of deterioration. In addition, temperature measurements made on coated and uncoated blades

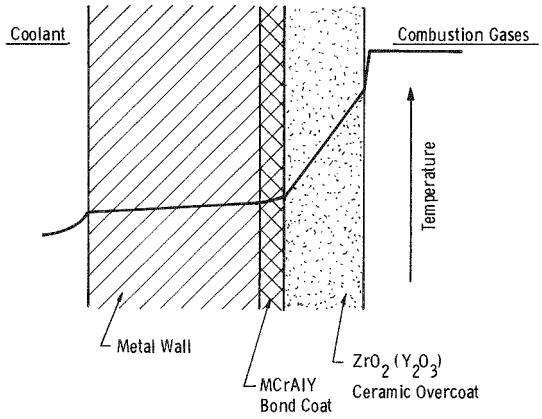

Figure 1-1 Schematic representation of the thermal barrier coating system.

during the engine tests corroborated the theoretically predicted insulating effect of the coating. Also, the coating system exhibited good adherence to blade and vane metals when cycled in a static burner rig 3200 times between 2340°F and 80°F and 275 times from 2714°F. However, preliminary hot corrosion tests (3) with sea salt injected into the flame at gas temperature of 1650°F indicated coating adherence problems after 300 h of operation.

Combustion tests (9) at the NASA-Lewis Research Center using a JT8D combustion liner with and without the ceramic thermal barrier coating, were most encouraging. With the thermal barrier coating, the maximum metal temperatures were reduced by 380°F with 10 mil thick yttria-stabilized zirconia outer layer over a 4 mil thick NiCrAlY bond coat, for a high aromatic fuel and a combustor exit temperature of 1925°F. For certain operating conditions, smoke and flame radiation were also decreased slightly compared to the uncoated liner.

Duplex thermal barrier coatings have also been investigated at the Linde Division of the Union Carbide Corporation. Tucker, et al. (10), have reviewed the development work conducted by the Linde Division. In their duplex thermal barrier coatings, both pre-alloyed and met-sealed* MCrAlY (M = Ni or Ni/Co) bond coats were used which were applied by plasma spraying using a proprietary inert gas shroud surrounding the plasma spray effluent. This inert gas shroud effectively eliminates any oxidation of the alloy as it is sprayed. The oxides used in their

*Met-sealed is a proprietary Union Carbide coating process that utilizes a mixture of powders rather than a single pre-alloyed composition.

work were yttria stabilized zirconia and magnesia-zirconia. The coatings were tested in isothermal and cyclic oxidation tests in air. From these tests, they concluded that in these duplex coatings, the bond coat must be effectively sealed to prevent any significant oxidation of the substrate or internal oxidation of the bond coat itself; the surface of the bond coat must be rough enough to provide an adherent surface for the oxide overcoat; and the oxide density must be controlled (to ~88% of theoretical density) for optimum thermal shock resistance.

In order to be used commercially, these thermal barrier coatings will have to successfully withstand, among other things, the corrosive environments of stationary gas turbines. This report summarizes the behavior of two duplex thermal barrier coating systems, one from the NASA-Lewis Research Center and the other from the Linde Division, both consisting of a MCrAlY (M = Ni or Ni/Co) bond coat and Y_2O_3-stabilized ZrO_2 overcoat, in several simulated gas turbine environments at 2000°F gas temperature. Initially, preliminary tests were conducted together with an on-going Westinghouse test program in order to obtain early results. The combustion environments were dictated by these in-house tests. The final tests conducted were planned to systematically determine the effects of sodium, vanadium and sulfur contaminants on the thermal barrier coating behavior. It should also be noted that a complete documentation of results in terms of photographs and post-test analyses is provided for future reference since this work is the first conducted of its kind on thermal barrier coatings.

Section 2

EXPERIMENTAL

THE EXPERIMENTAL EQUIPMENT

The behavior of duplex thermal barrier coating systems has been studied in a pressurized turbine test passage which simulates the operational environment of a stationary gas turbine. Figure 2-1 shows a schematic diagram of this test facility, wherein, air compressed to about 100 lb/in^2 is preheated in an indirectly fired air heater to 600°F and fed into a Hastelloy-X combustor. Fuel is injected into the primary combustion zone through a bayonet-mounted fuel nozzle in the dome-shaped front portion of the combustor and burned with a compressed air. Combustion gases are then mixed with secondary cooling air, the amount of which is adjusted to attain the desired gas temperature. At the combustor exit, an array of 16 thermocouples measures the temperature of the combustion gases.

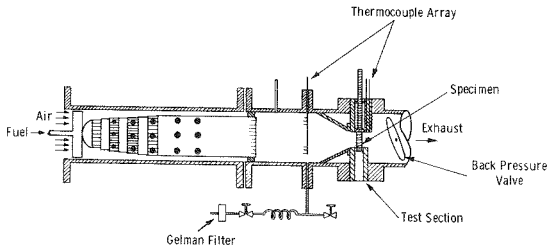

Figure 2-1 High temperature pressurized turbine test passage.

Downstream of the thermocouple array, a transition section reduces the flow area and increases the gas velocity to ∿500 fps. At this location, the coated specimens are exposed to the high velocity hot combustion gases. A test section holds a set of eight 0.25 in. diameter uncooled solid cylindrical pins, or two air-cooled cylindrical sleeves 1.0 in. diameter and 2.0 in. long (Figure 2-2). These

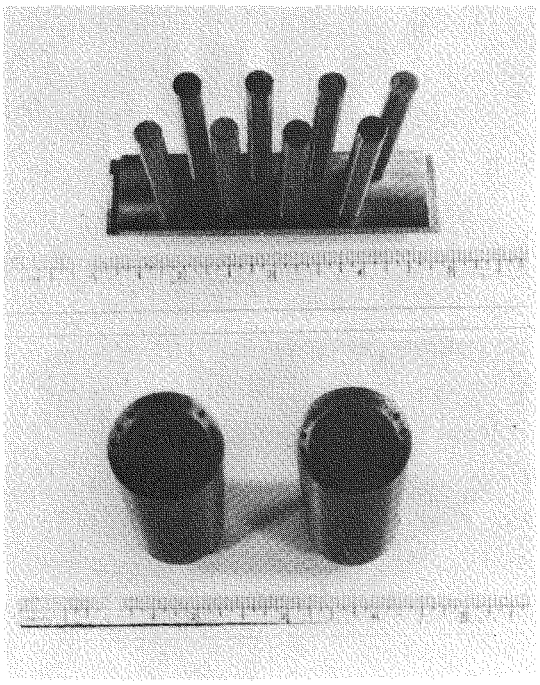

Figure 2-2 0.25 in. diameter solid pins for uncooled tests (top); 1.0 in. diameter cylindrical sleeves for cooled tests (bottom).

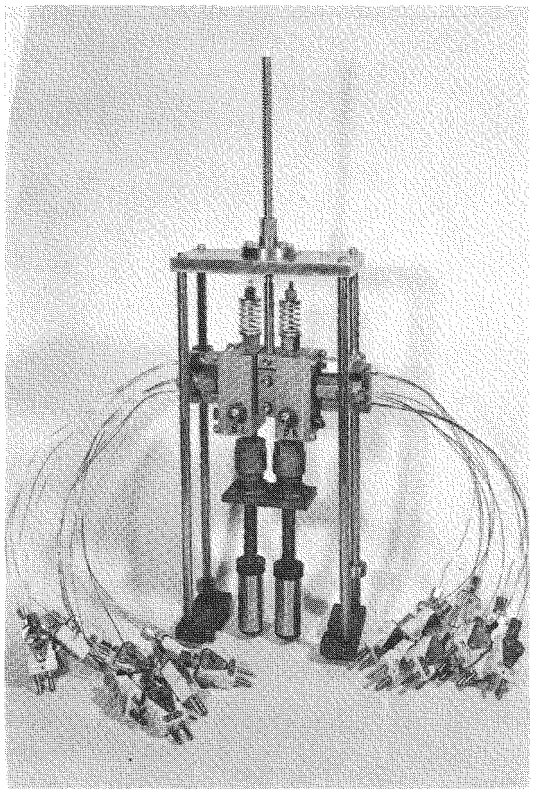

Figure 2-3 Cooled specimen assembly.

cylindrical sleeves have 12 holes drilled lengthwise to various depths to accommodate thermocouples which measure the metal surface temperature. Cooling air is passed through the inside of the sleeves to achieve the desired metal temperature. The cooled specimen assembly is shown in Figure 2-3. At the other end of the test section, a water-cooled barrier plate acts as a damper valve and maintains a pressure of 3 atm in the passage. The exhaust gases are cooled by a water spray and vented to the atmosphere through an extensive muffler system to reduce noise to acceptable levels.

The basic fuel used for the experiments described in this report was No. GT-2 diesel oil (Exxon 260). A typical chemical analysis of this fuel is shown in Table 2-1. The levels of sulfur, sodium and vanadium in the fuel were increased to desired levels by mixing in appropriate amounts of the following compounds in the fuel oil:

Sulfur: Ditertiary butyl disulfide
Sodium: Sodium napthenate
Vanadium: Vanadium carboxylate

In a typical test run, the temperature of the combustion gases was gradually increased in ∿1 h to the desired gas temperature. During this heat-up, the specimens were kept away from the combustion gases and experienced temperatures of 500°-600°F. After the combustion gases reached the desired temperature, the specimens were lowered in the gas stream (within ∿1 min) and exposed isothermally to the combustion gases. After 8 to 10 h, the specimens were retracted away from the gas stream (within ∿1 min) and then the fuel cut-off gradually to complete shutdown in ∿5 min. The specimens cooled down to the room temperature in 30 min. In this fashion, the testing was continued from day to day to accumulate the desired exposure time on the specimens. Thus, even though no thermal cycling of the specimens was intended, the specimens did experience one heat-up and cool-down cycle for every 8-10 h of exposure.

Table 2-1

TYPICAL CHEMICAL ANALYSIS OF NO. GT-2
DIESEL OIL (EXXON 260)

Element	Concentration (ppm)
Fe	2.0
Cu	0.8
Si	0.8
Mn	0.6
Pb	0.5
Al	0.3
Mg	0.3
Na and K	0.3
P	0.3
Ca	0.2
Cr	0.2
V	0.7
S	0.242 (wt%)

Following exposure to combustion gases in the pressurized turbine test passage, the specimens were weighed, measured and examined visually and optically. The specimens were then analyzed in detail by metallography, X-ray diffraction and electron microprobe analyses. However, even though all the specimens were weighed and measured before and after exposure to combustion gases, these measurements were not found to be of much value because of uneven attack (spalling, chipping, etc.) and formation of deposits on the surface of the specimens from the combustion gases. The data on weight and dimensional changes, therefore, is not discussed in this report. The most valuable information was obtained by metallography, X-ray diffraction and electron microprobe analyses.

THE COATING SYSTEMS

The duplex coatings consisting of a MCrAlY (M = Ni or Ni/Co) bond coat and the Y_2O_3-stabilized ZrO_2 overcoat on Udimet-500 specimens were obtained from two sources:

- NASA-Lewis Research Center
- Union Carbide Corp. - Linde Division

Both the bond coat and the oxide overcoat in each of the coating systems were deposited by plasma spraying. The Linde coating was deposited using an inert gas shroud surrounding the plasma spray effluent in order to eliminate any oxidation of the bond coat alloy powder as it was sprayed. No such protective shield was used by NASA in depositing the coatings.

The NiCrAlY/$ZrO_2(Y_2O_3)$ Coating from NASA

The bond coat in the NASA coating had a nominal composition of 16 wt% Cr, 5 wt% Al, 0.6 wt% Y and the balance Ni, while the overcoat was ZrO_2 stabilized with nominally 12 wt% Y_2O_3. Detailed chemical analysis of the oxide overcoat is shown in Table 2-2. Metallographic cross-sections of a typical NASA coating are shown in Figures 2-4 and 2-5. The bond coat in these coatings was found to vary from ∿0.5 to 4 mil in thickness around the circumference of the specimen, and at a few points, there was practically no bond coat present. The $ZrO_2(Y_2O_3)$ oxide overcoat was relatively uniform in thickness, ∿14 mil. The surface roughness of this oxide overcoat averaged ∿400 μin., rms.

The oxide overcoat was found by X-ray diffraction analysis to contain only the cubic $ZrO_2(Y_2O_3)$ phase with lattice parameter equal to 5.1367 Å. The electron microprobe scans revealed the presence of large inclusions of alumina in the

Table 2-2

CHEMICAL ANALYSIS OF THE OXIDE OVERCOAT IN NASA AND LINDE THERMAL BARRIER COATING

	Concentration wt%	
Element	NASA	Linde
ZrO_2	85.78 (± 0.5)	87.30 (± 0.5)
Y_2O_3	13.30 (± 0.5)	11.45 (± 0.5)
Si	0.2	0.02
Al	0.02	0.2
Fe	0.1	0.1
Mg	0.03	0.008
Ni	0.02	0.03
Ti	0.06	0.03
V	0.01	0.01
Cr	0.01	0.02
Hf	1.0	not detectable
Yb	detectable[a]	detectable

[a] Yb about 10 times greater in the NASA coating than in the Linde coating.

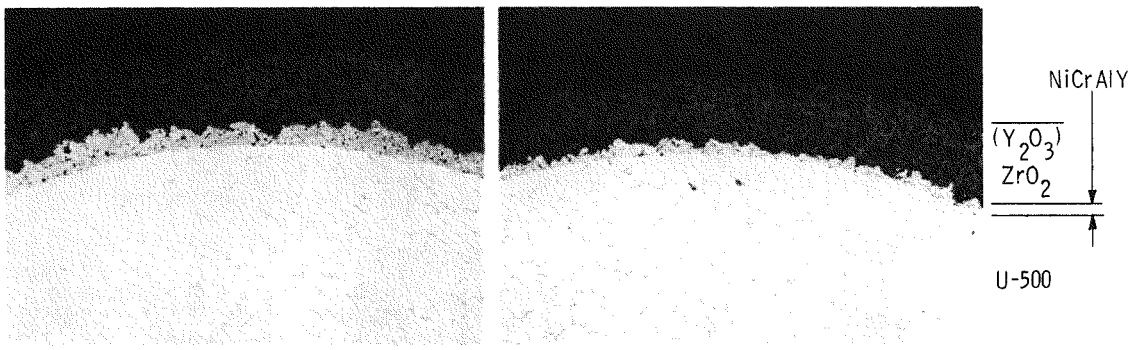

Figure 2-4 Metallographic cross sections of the NASA coating showing non-uniformity of the NiCrAlY bond coat (50 X).

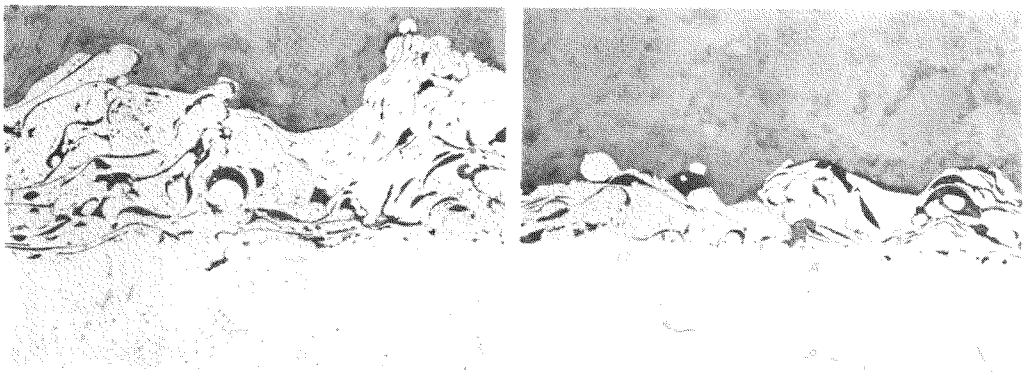

Figure 2-5 Metallographic cross-sections of the NASA coating showing details of the NiCrAlY bond coat (500 X).

NiCrAlY bond coat; these inclusions appear as dark regions in the metallographic cross-sections shown in Figure 2-5. The electron microprobe scans also revealed the presence of a minor second phase in the $ZrO_2(Y_2O_3)$ overcoat. This phase consisted mainly of yttrium and silicon, possibly yttrium silicate.

The NiCoCrAlY/$ZrO_2(Y_2O_3)$ Coating from Linde Division

The bond coat in the Linde coating consisted of a cobalt-base alloy with 32 wt% Ni, 21 wt% Cr, 7.5 wt% Al and 0.5 wt% Y, while the overcoat was again ZrO_2 stabilized with nominally 12 wt% Y_2O_3. Detailed chemical analysis of the oxide overcoat is shown in Table 2-2. The metallographic cross-section of a typical Linde coating is shown in Figure 2-6. Both the bond coat and the oxide overcoat

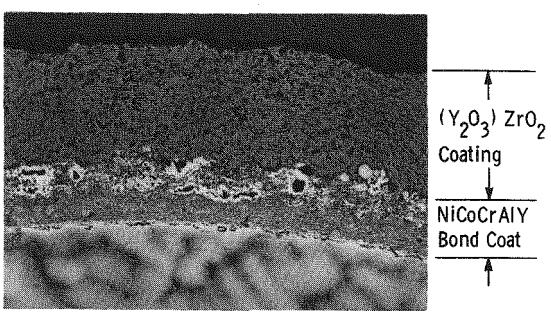

Figure 2-6 Metallographic cross-section of the Linde coating showing the bond coat and the oxide overcoat (100 X).

in the Linde coatings were found to be fairly uniform in thickness; the bond coat being ∿6.5 mil and the oxide overcoat ∿12 mil in thickness. The surface roughness of the coating averaged 240 μin., rms.

X-ray diffraction analysis revealed the oxide overcoat to be predominantly a tetragonal $ZrO_2(Y_2O_3)$ phase with the following lattice parameters:

a = 5.1232 Å

c = 5.1528 Å

The oxide overcoat possibly also contained the cubic $ZrO_2(Y_2O_3)$ phase; its determination was made difficult and rather uncertain because the lattice parameters of the tetragonal and cubic phases differ only very slightly. Also, in contrast to the NASA coating, the electron microprobe scans indicated the absence of any alumina inclusions in the bond coat or any yttrium silicate in the oxide overcoat.

Section 3

TEST RESULTS

PRELIMINARY TESTS - UNCOOLED SOLID TEST SPECIMENS

The experimental conditions under which uncooled coated specimens were tested and the coating condition after the test are summarized in Table 3-1. The particular experimental condition employed were dictated by the in-house Westinghouse experiments on other materials being conducted at the time of these tests. The tests are described in detail below.

Table 3-1

SUMMARY OF EXPERIMENTS WITH UNCOOLED SOLID SPECIMENS

Test Parameters		Coating Type	Total Test Time	Coating Condition After Test
Gas Temp.	Fuel Additives			
1650°F	5 ppm Pb 0.5 wt% S	NASA	101 h	No Spalling
1650°F	3 ppm Na 5 ppm V 0.5 wt% S	NASA Linde	62 h	Chipped and spalled
1800°F	10 ppm Na 18 ppm Cl 1.5 ppm Mg 0.5 wt% S	NASA Linde	78 h 87 h	Chipped and spalled
1650°F	0.5 ppm Na 10 ppm V 0.5 wt% S	NASA	42 h	Chipped and spalled

Test with 5 ppm Pb in the Fuel

One NASA-coated solid cylindrical pin was exposed at 1650°F to hot combustion gases obtained by burning GT-2 diesel oil with 5 ppm Pb and 0.5 wt% S. The oxide coating on the exposed specimen remained intact and free of any macrocracking or spalling even after 101 h of exposure. The surface of the exposed specimen after 101 h of exposure is shown in Figure 3-1 along with an as-coated untested specimen. A metallographic cross-section of the exposed specimen is shown in Figure 3-2 which indicates no microcracking of the oxide coating either. The coating surface did pick up small amounts of deposits from the combustion gases during exposure and showed a net weight gain of 11.6 mg in 101 h. These deposits were identified by X-ray diffraction analysis to be predominantly barium sulfate ($BaSO_4$). Barium was a constituent of the fuel used in this particular test, added by the fuel manufacturer to prevent gum formation during fuel storage and to reduce excessive smoke formation on combustion. The electron microprobe scans for Zr, Y, Si, Pb, P and S from the surface of the specimen after exposure to combustion gases are shown in Figure 3-3. These scans reveal the presence of minor amounts of sulfur and phosphorous, but indicate no Pb at the surface. Also apparent are Y + Si regions in the oxide coating, which are present in the as-received NASA-coated specimens.

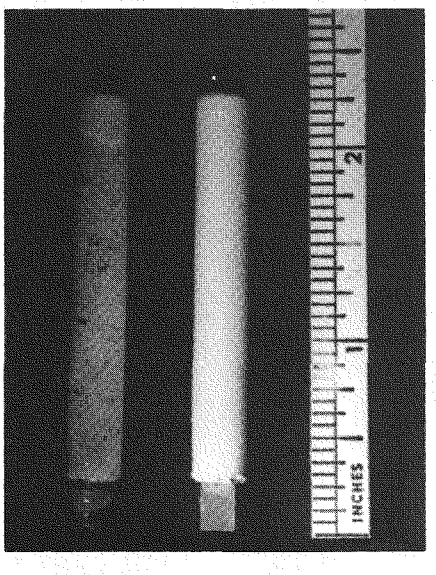

Figure 3-1 The NASA-coated specimen before (right) and after (left) 101 h of exposure at 1650°F with 5 ppm Pb in the fuel.

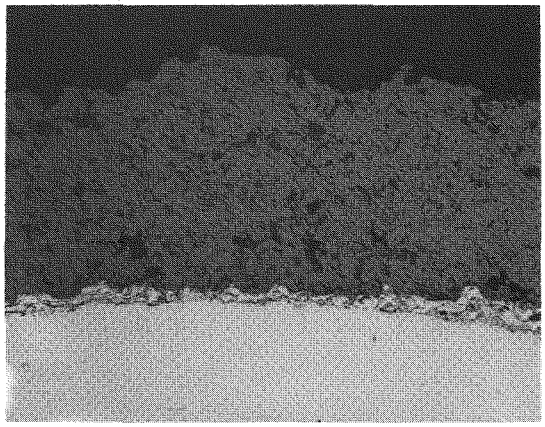

Figure 3-2 Metallographic cross-section of the NASA-coated specimen after 101 h of exposure at 1650°F with 5 ppm Pb in the fuel (100 X).

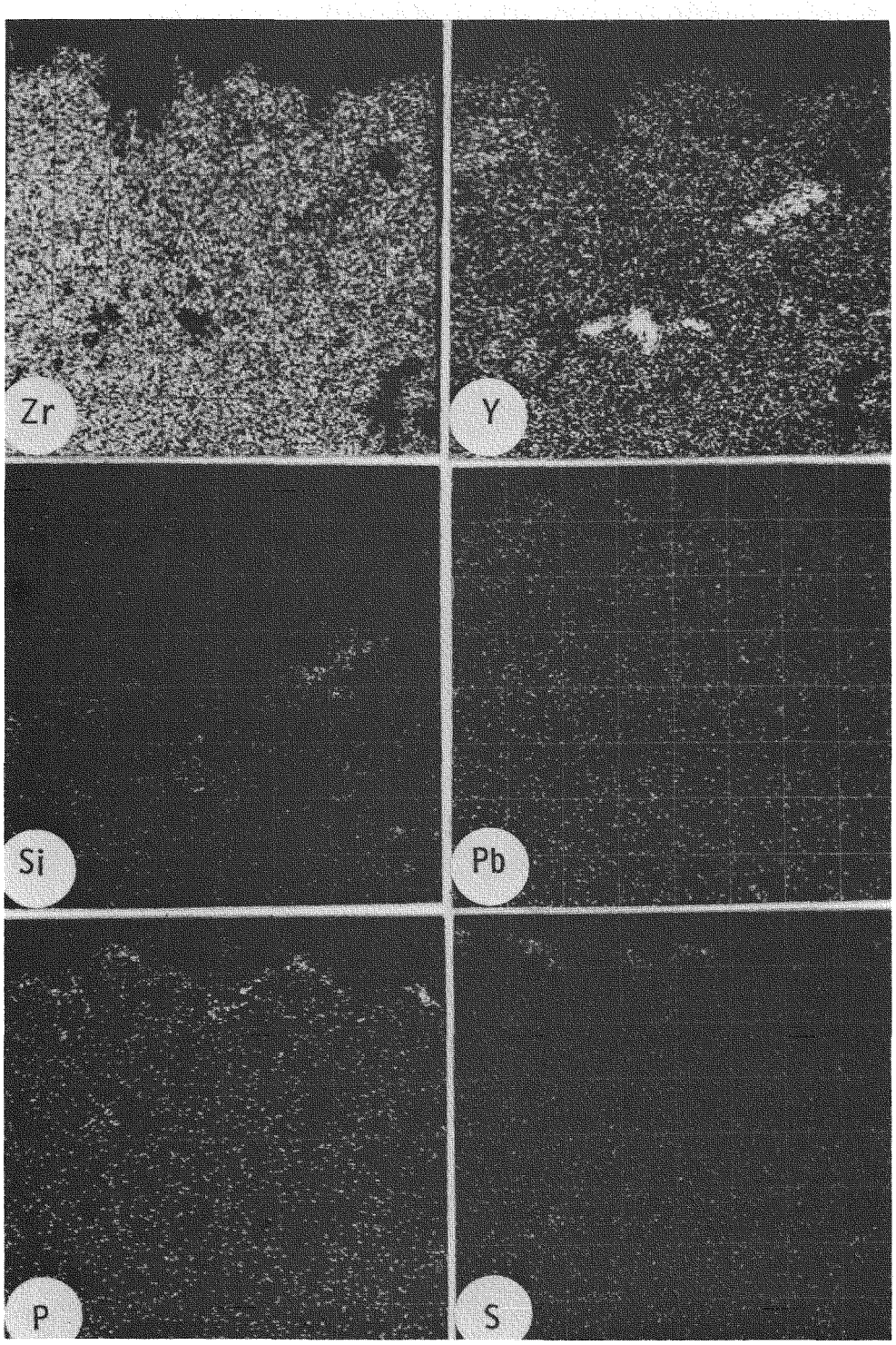

Figure 3-3 Electron microprobe scans from the NASA-coated specimen after 101 h of exposure at 1650°F with 5 ppm Pb in the fuel.

Test with 3 ppm Na and 5 ppm V in the Fuel

One each NASA- and Linde-coated specimen was exposed to hot combustion gases at 1650°F using GT-2 diesel oil doped with 3 ppm Na, 5 ppm V and 0.5 wt% S. The surface appearance of these exposed specimens (four views of each specimen) are illustrated in Figures 3-4 and 3-5, which show that the oxide coating on both the NASA- and the Linde-coated specimens severely chipped and spalled off very early during the exposure. The oxide coating on the NASA-coated specimen was almost completely gone at 62 h of exposure, while that on the Linde-coated specimen lasted only 31 h of exposure. Figures 3-6 and 3-7 show the metallographic cross-sections of the exposed NASA- and Linde-coated specimens respectively. The oxide coating appears to have spalled off from within its own thickness, and there is still some $ZrO_2(Y_2O_3)$ oxide left at the MCrAlY/$ZrO_2(Y_2O_3)$ interface. The coated surfaces of the exposed specimens contained significant amounts of V and P, in addition to minor amounts of Na and S, as shown in the electron microprobe scans in Figure 3-8. X-ray diffraction analysis identified following phases in the surface after exposure: $ZrO_2(Y_2O_3)$ (tetragonal/cubic) (major); ZrO_2 (monoclinic) (minor); YPO_4 (minor); $NaZr_2(PO_4)_3$ (minor); α-Fe_2O_3 (minor); and spinel (minor). No vanadium compound was detected by the x-ray diffraction analysis.

Figure 3-4 NASA-coated specimen after 62 h of exposure at 1650°F with 3 ppm Na and 5 ppm V in the fuel.

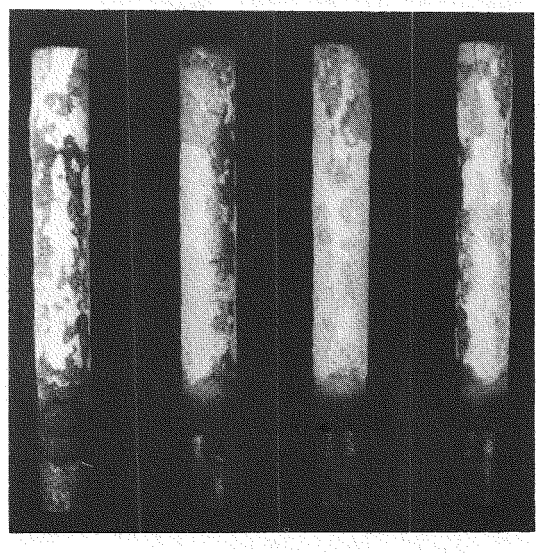

Figure 3-5 Linde-coated specimen after 31 h of exposure at 1650°F with 3 ppm Na and 5 ppm V in the fuel.

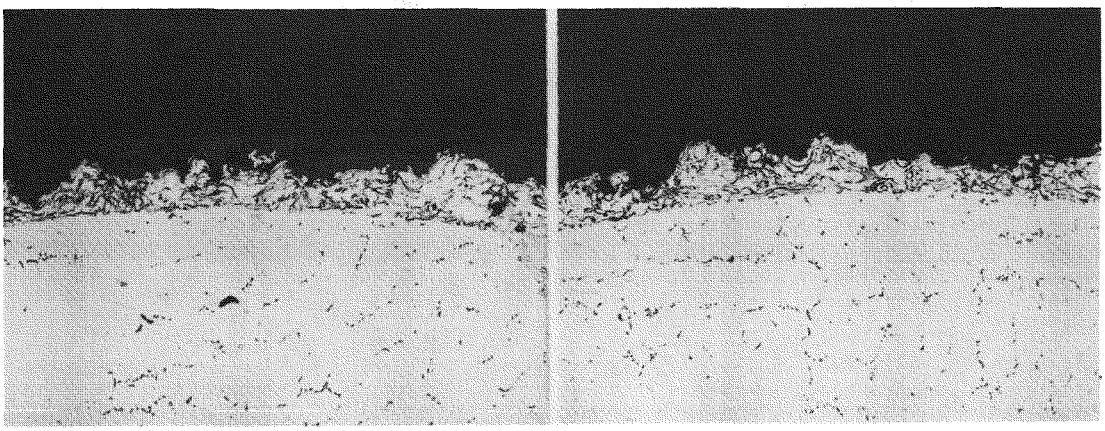

Figure 3-6 Metallographic cross-section of the NASA-coated specimen after 62 h of exposure at 1650°F with 3 ppm Na and 5 ppm V in the fuel (100 X).

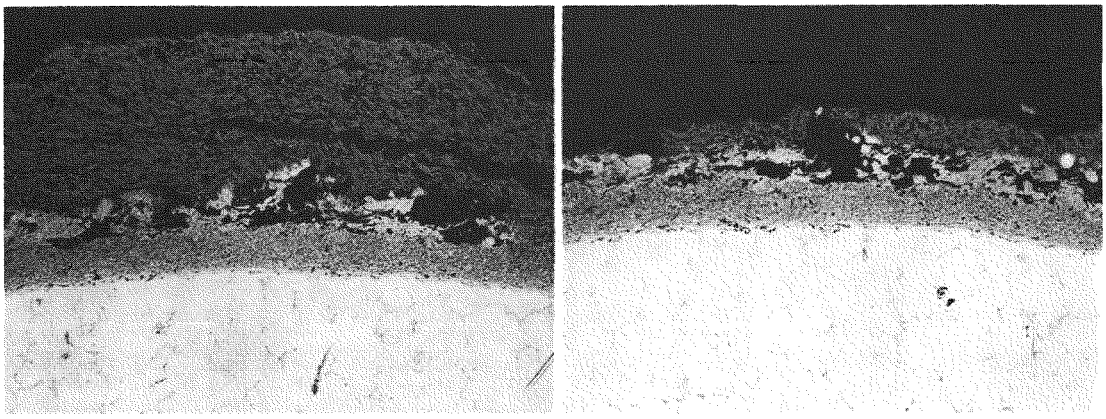

Figure 3-7 Metallographic cross-section of the Linde-coated specimen after 31 h of exposure at 1650°F with 3 ppm Na and 5 ppm V in the fuel (100 X).

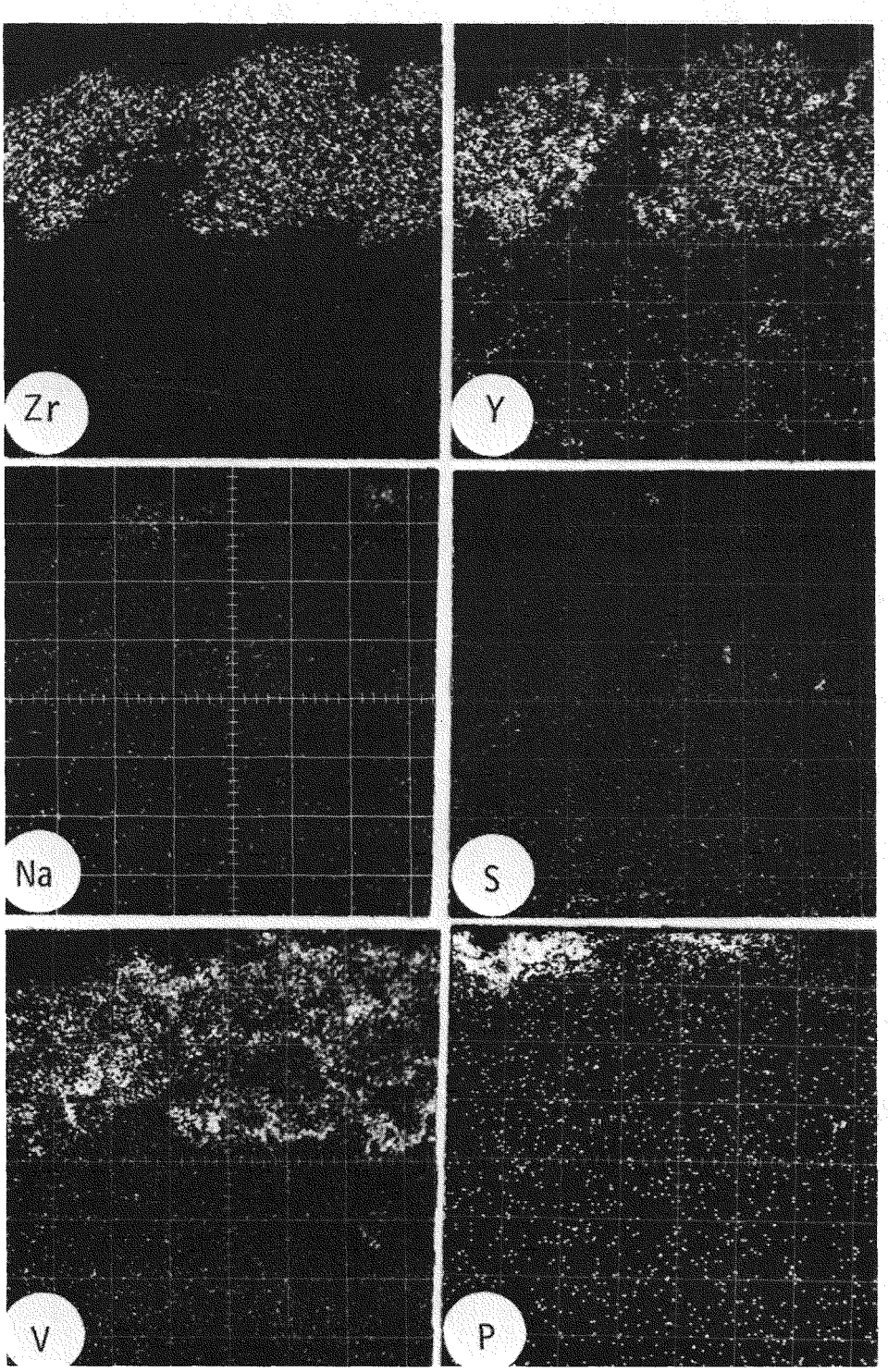

Figure 3-8 Electron microprobe scans from the Linde-coated specimen after 31 h of exposure at 1650°F with 3 ppm Na and 5 ppm V in the fuel.

Test with 10 ppm Na, 18 ppm Cl and 1.5 ppm Mg in the Fuel

One each NASA- and Linde-coated specimen was exposed to 1800°F to hot combustion gases obtained by burning GT-2 diesel oil doped with 10 ppm Na, 18 ppm Cl, 1.5 ppm Mg and 0.5 wt% S. The oxide coating on the NASA-coated specimen severely cracked and appeared to have separated from the specimen after 78 h of exposure as shown in Figure 3-9. A metallographic cross-section of the specimen after this 78 h of exposure is shown in Figure 3-10, which reveals that the coating separated from the NiCrAlY bond coat. However, no corrosion of this bond coat was apparent or detected by oxygen electron microprobe analysis.

The oxide coating on the Linde-coated specimen also chipped and spalled off in small pieces and was almost completely removed from some regions of the specimen surface in 87 h of exposure to the hot combustion gases. The surface appearance of the Linde-coated specimen (four views of the specimen) after 87 h of exposure is shown in Figure 3-11. The metallographic cross-sections from two different

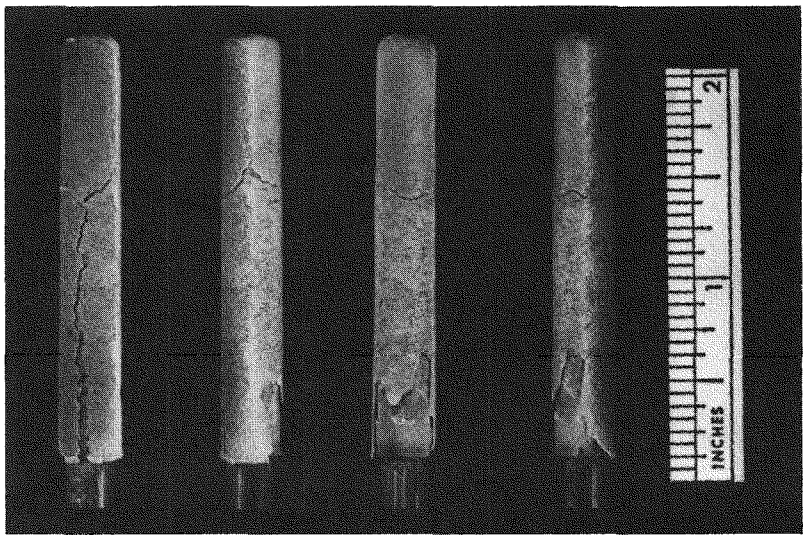

Figure 3-9 NASA-coated specimen after 78 h of exposure at 1800°F with 10 ppm, 18 ppm Cl and 1.5 ppm Mg in the fuel.

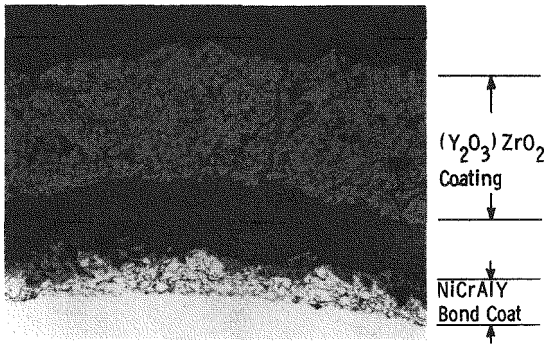

Figure 3-10 Metallographic cross-section of the NASA-coated specimen after 78 h of exposure at 1800°F with 10 ppm Na, 18 ppm Cl and 1.5 ppm Mg in the fuel (100 X).

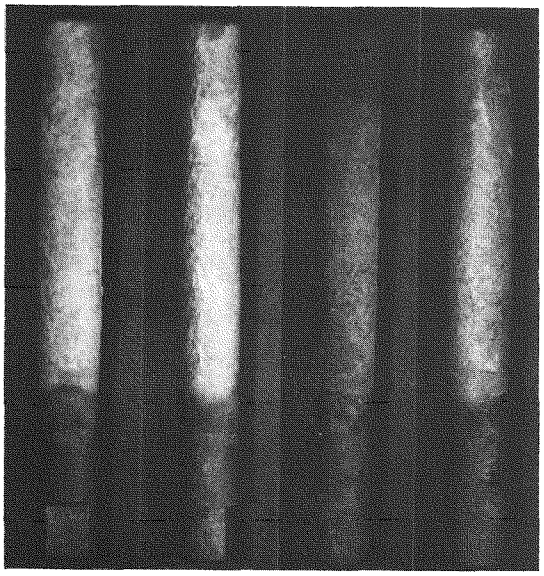

Figure 3-11 Linde-coated specimen after 87 h of exposure at 1800°F with 10 ppm Na, 18 ppm Cl and 1.5 ppm Mg in the fuel

regions of the exposed specimen, shown in Figure 3-12, revelaed that the oxide coating in this case did not separate from the bond coat but rather cracked and chipped off within its own thickness.

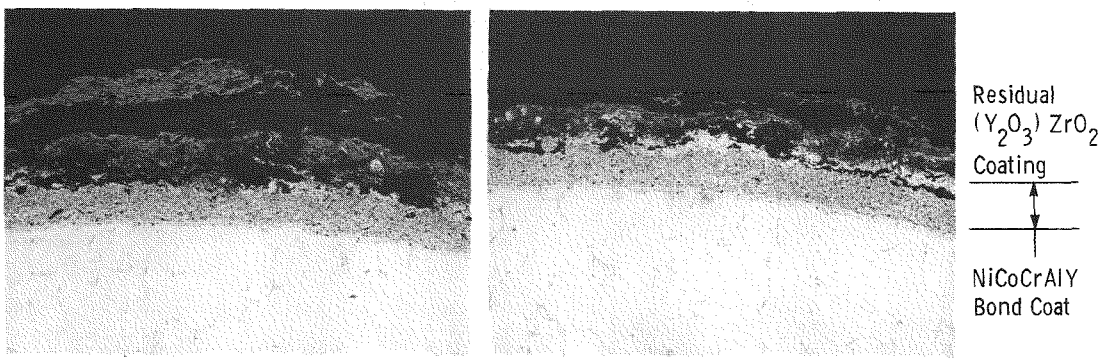

Figure 3-12 Metallographic cross-sections from two regions of the Linde-coated specimen after 87 h of exposure at 1800°F with 10 ppm Na, 18 ppm Cl and 1.5 ppm Mg in the fuel (100 X).

The electron microprobe scans for Zr, Y, Na, Cl, Mg and P from the surface of an exposed specimen are shown in Figure 3-13. These reveal that Na, Cl and P

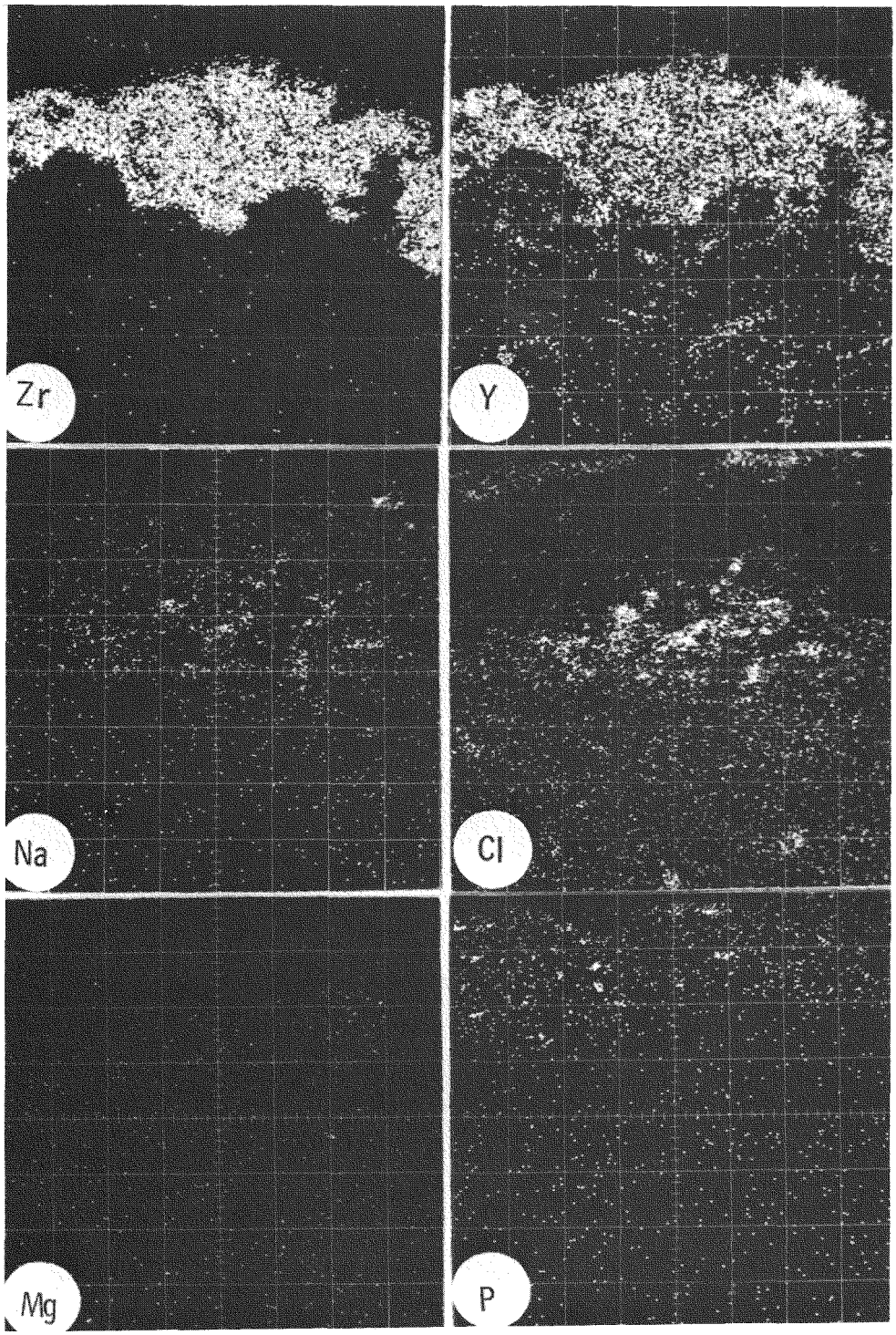

Figure 3-13 Electron microprobe scans from the NASA-coated specimen after 78 h of exposure at 1800°F with 10 ppm Na, 18 ppm Cl and 1.5 ppm Mg in the fuel.

from the combustion gases have penetrated through the oxide overcoat. X-ray diffraction analysis identified $ZrO_2(Y_2O_3)$ (tetragonal/cubic)(major), ZrO_2 (monoclinic) (minor), YPO_4 (minor), and spinel (minor) in the surface of the exposed specimens.

Test with 0.5 ppm Na and 10 ppm V in the Fuel

A NASA-coated specimen was exposed to hot combustion gases at 1650°F using GT-2 diesel oil doped with 0.5 ppm Na, 10 ppm V and 0.5 wt% S. The surface appearance of the specimen after 42 h of exposure, and metallographic cross-sections from two different regions of the exposed specimen, are shown in Figures 3-14 and 3-15, respectively. These show that the oxide coating spalled off almost completely from the front of the specimen. Electron microprobe scans, Figure 3-16, indicated minor amounts of P in the exposed oxide coating. X-ray diffraction analysis

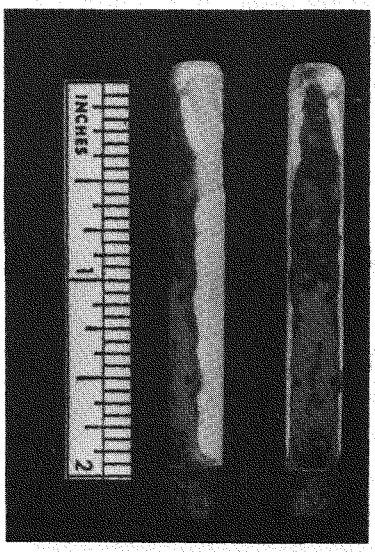

Figure 3-14 Two views of NASA-coated specimen after 42 h of exposure at 1650°F with 0.5 ppm Na and 10 ppm V in the fuel.

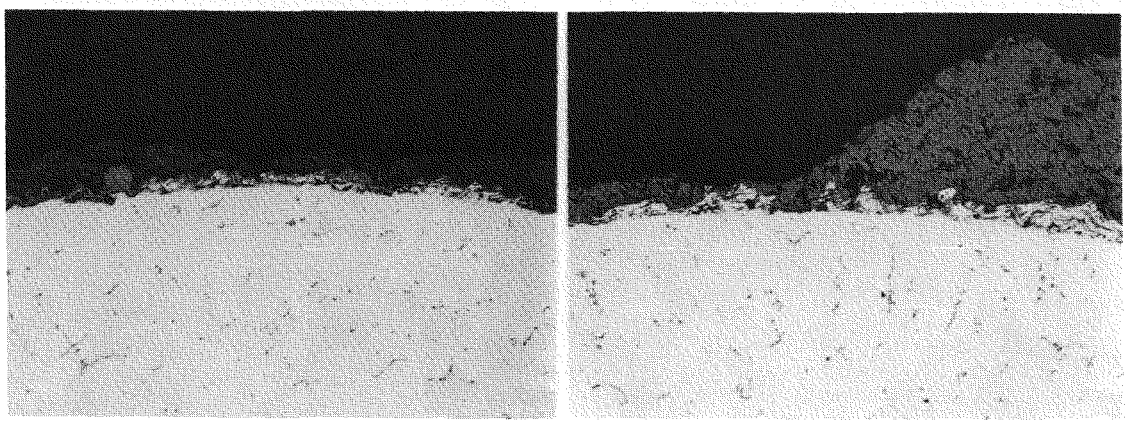

Figure 3-15 Metallographic cross-sections from two different regions of the NASA-coated specimen after 42 h of exposure at 1650°F with 0.5 ppm Na and 10 ppm V in the fuel (100 X).

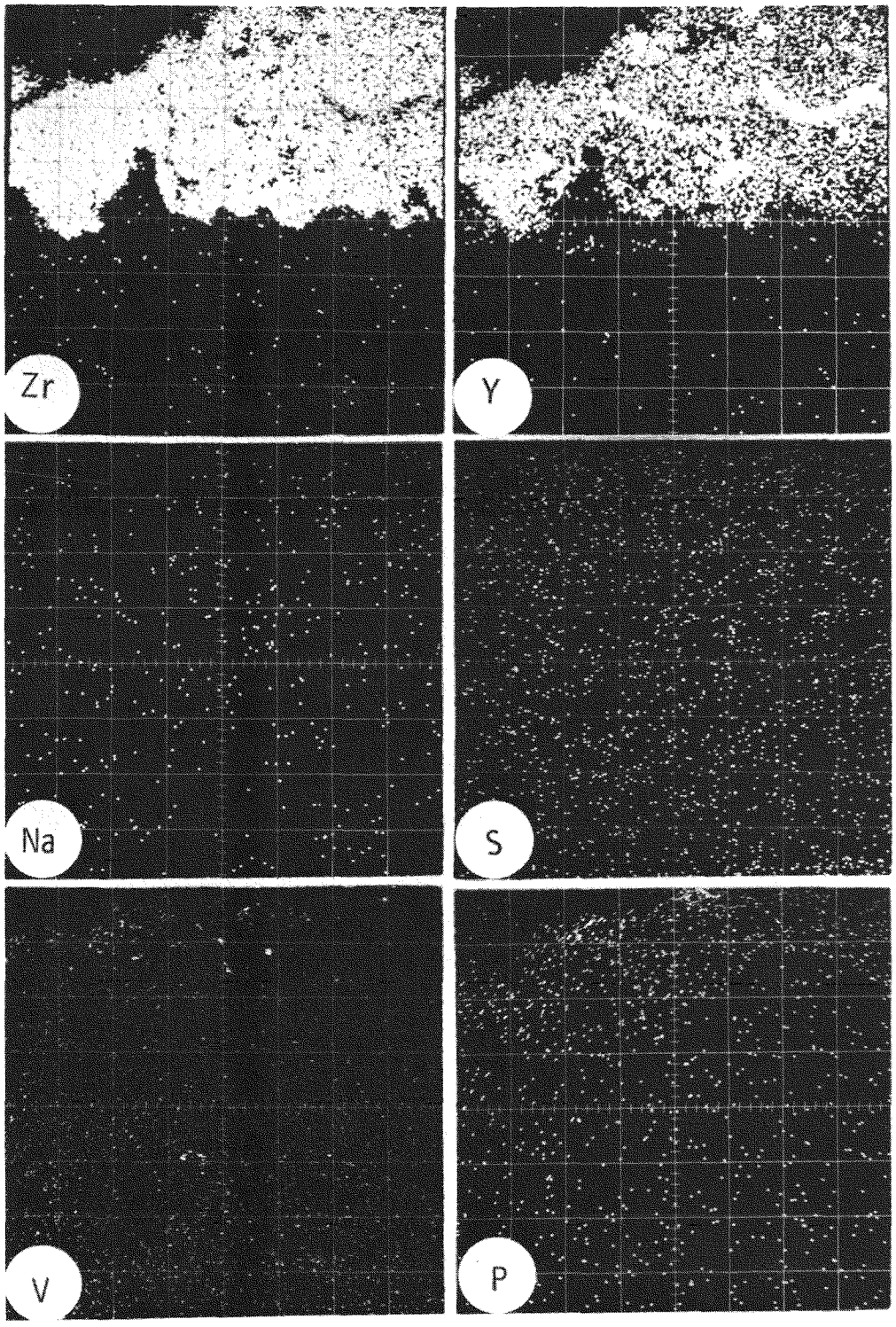

Figure 3-16 Electron microprobe scans from the NASA-coated specimen after 42 h of exposure at 1650°F with 0.5 ppm Na and 10 ppm V in the fuel (100 X).

detected the following phases in the surface of the exposed specimen: $ZrO_2(Y_2O_3)$ (tetragonal/cubic)(major); ZrO_2 (monoclinic)(minor); $NaZr_2(PO_4)_3$ (minor); YPO_4 (minor) and $BaSO_4$ (minor). Barium was present in the fuel used for this particular test. Again, no vanadium compound was detected in the exposed surface oxide coating.

PRELIMINARY TESTS - COOLED TEST SPECIMENS

Initially, two cooled tests were run on both NASA- and Linde-coated specimens using GT-2 diesel fuel doped with 5 ppm Na, 2 ppm V, and 0.5 wt% S at a gas temperature of 2000°F. These two tests are described below:

Test 1 with 5 ppm Na, 2 ppm V and 0.5 wt% S in the Fuel

In the first test, one NASA-caoted specimen and one uncoated Udimet-500 specimen were exposed to the hot combustion gases at 2000°F. Both specimens were air-cooled to keep the average metal temperature at ∿1500°F. The maximum and minimum temperatures experienced by different regions of the metal surface of the NASA-coated specimen during the course of the test are shown in Figure 3-17. This

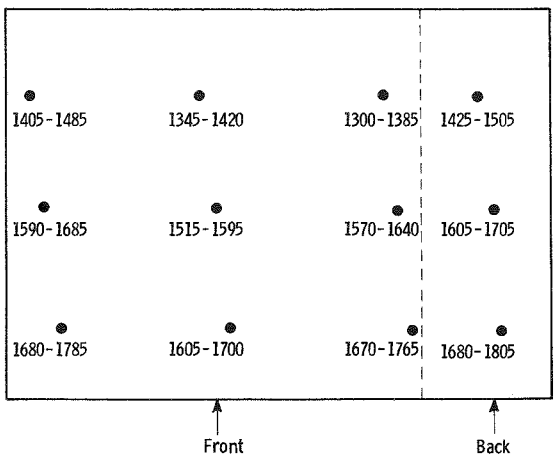

Figure 3-17 Temperatures (in °F) at the metal surface of the NASA-coated air-cooled specimen in the pressurized turbine test passage at 2000°F gas temperature.

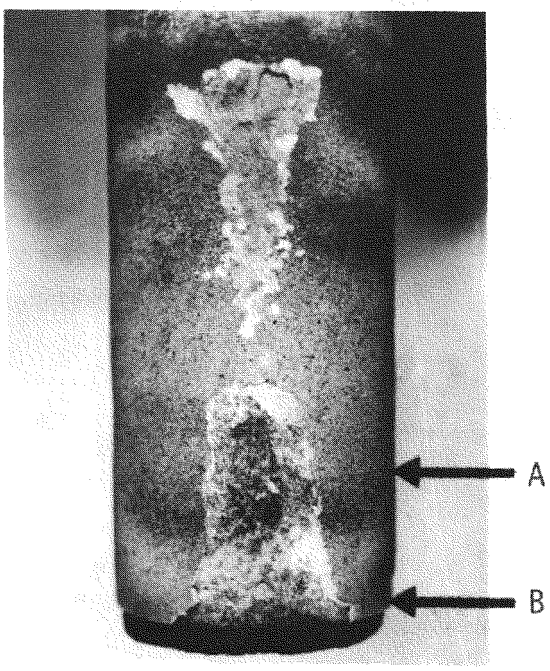

Figure 3-18 Front view of the NASA-coated specimen after 46.5 h of exposure at average metal surface temperature of 1500°F with 5 ppm Na, 2 ppm V and 0.5 wt% S in the fuel.

temperature profile shows that some regions of the metal surface experienced temperatures as high as 1805°F during the course of the test. The NASA-coated specimen started exhibiting some spalling of the oxide coating as early as 21 h of exposure to combustion gases, and the amount of spalling increased with increasing exposure time. The front surface of the specimen after 46.5 h of exposure is shown in Figure 3-18. The amount of oxide spalling was observed to be greatest in the bottom front of the specimen, which is the region of the highest metal surface temperature. The metallographic cross-sections from four different regions around the circumference of the specimen are shown in Figures 3-19 and 3-20. At about 0.5 in. from the bottom of the specimen (Location A in Figure 3-18) the metallographic cross-sections (Figure 3-19) show that the oxide coating separated from the NiCrAlY bond coat both at the front and the right side of the specimen. However, the coating did remain intact on the backside of the specimen. At the bottom of the specimen (Location B in Figure 3-18), however, not only the oxide coating spalled off completely throughout the circumference of the specimen, but some NiCrAlY bond coat also spalled off (Figure 3-20). As a result of this removal of NiCrAlY bond coat, severe corrosion of the Udimet-500 substrate has occurred.

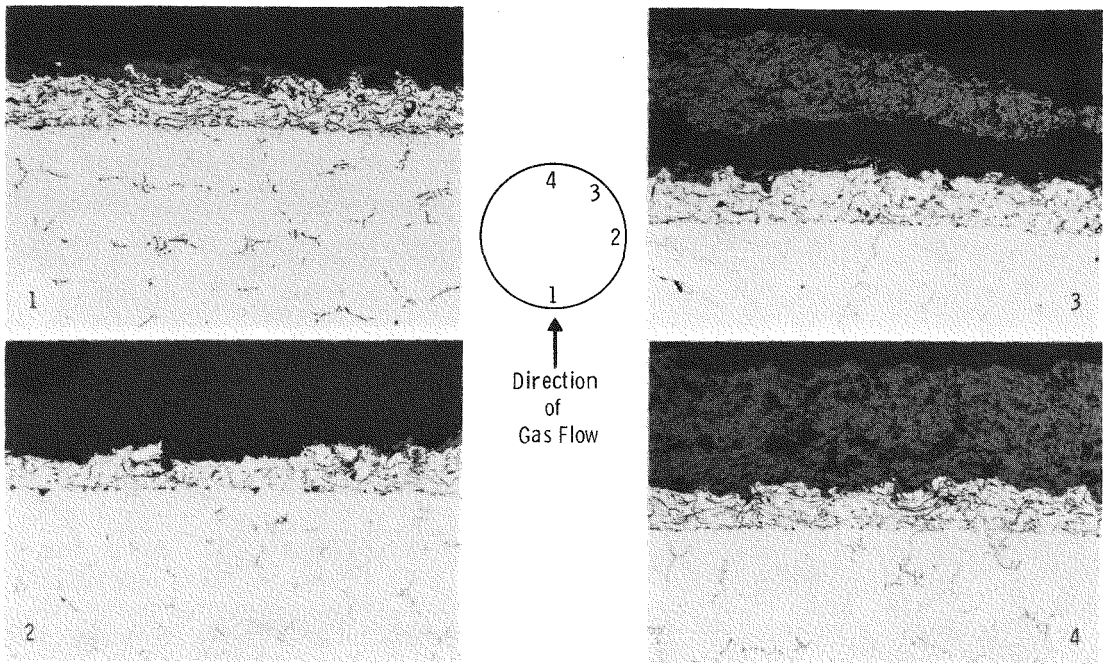

Figure 3-19 Metallographic cross-sections of the NASA-coated specimen after 46.5 h of exposure; location A in Figure 3-18 (100 X).

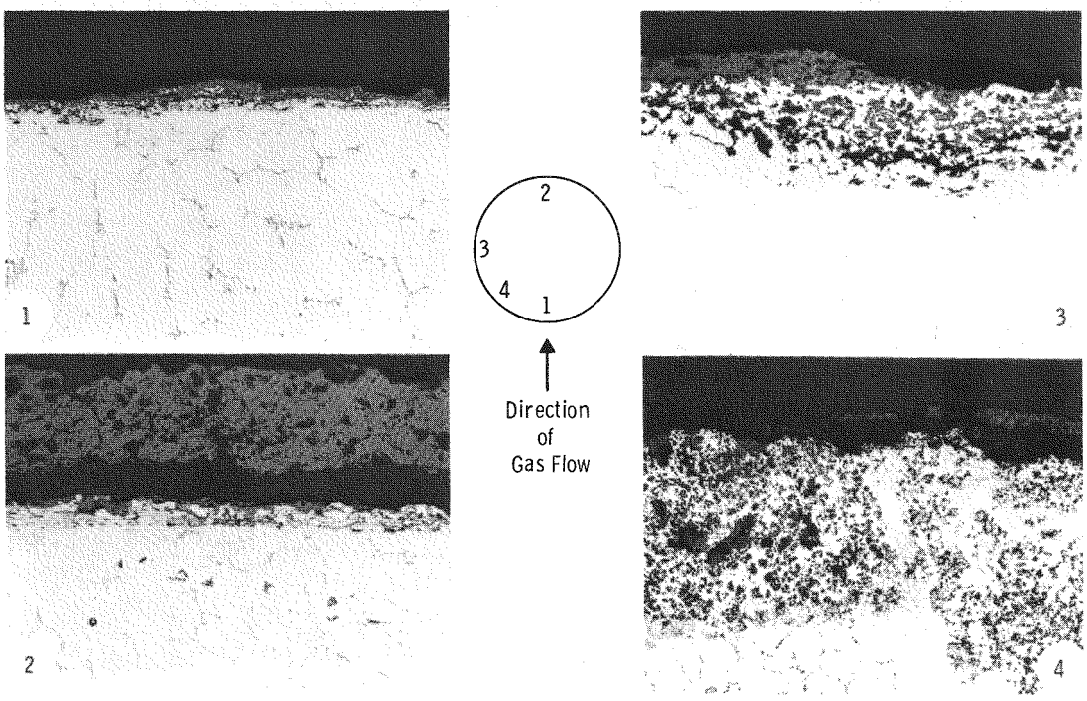

Figure 3-20 Metallographic cross-sections of the NASA-coated specimen after 46.5 h of exposure; location B in Figure 3-18 (100 X).

Test 2 with 5 ppm Na, 2 ppm V and 0.5 wt% S in the Fuel

The second cooled test, on both NASA- and Linde-coated specimens, was also run at 2000°F gas temperature using the same fuel and additives, but the amount of cooling air was increased to keep the metal surface temperature to a maximum of 1650°F. This resulted in an average metal surface temperature of ∿1450°F. The maximum and minimum temperatures expeirenced by different regions of the metal surface of the NASA- and the Linde-coated specimens are shown in Figure 3-21.

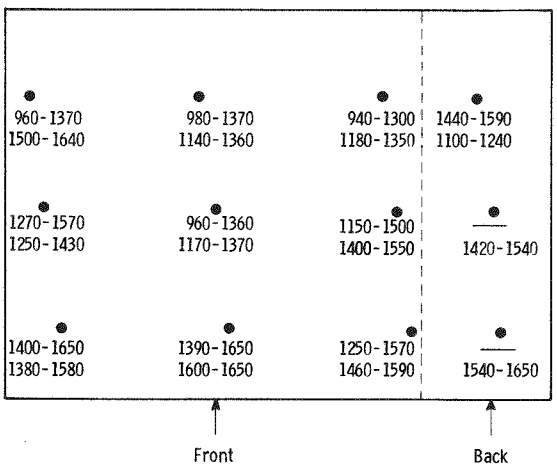

Figure 3-21 Temperatures (in °F) at the metal surface of the air-cooled specimens in the pressurized turbine test passage at 2000°F gas temperature. Linde-coated specimen: top number; NASA-coated specimen: bottom number.

After 37 h of exposure, the oxide coating on the NASA-coated specimen was found intact while that on the Linde-coated specimen experienced some spalling. However, with further exposure to a total of 63.5 h, the NASA coating also showed oxide spalling while the amount of oxide spalling increased on the Linde-coated specimen. The severe spalling on the NASA- and Linde-coated specimens is illustrated in Figures 3-22 and 3-23 for four views of each specimen. The metallographic cross-sections for four different locations around the circumference of the exposed specimens are shown in Figures 3-24 and 3-25. These reveal that numerous cracks

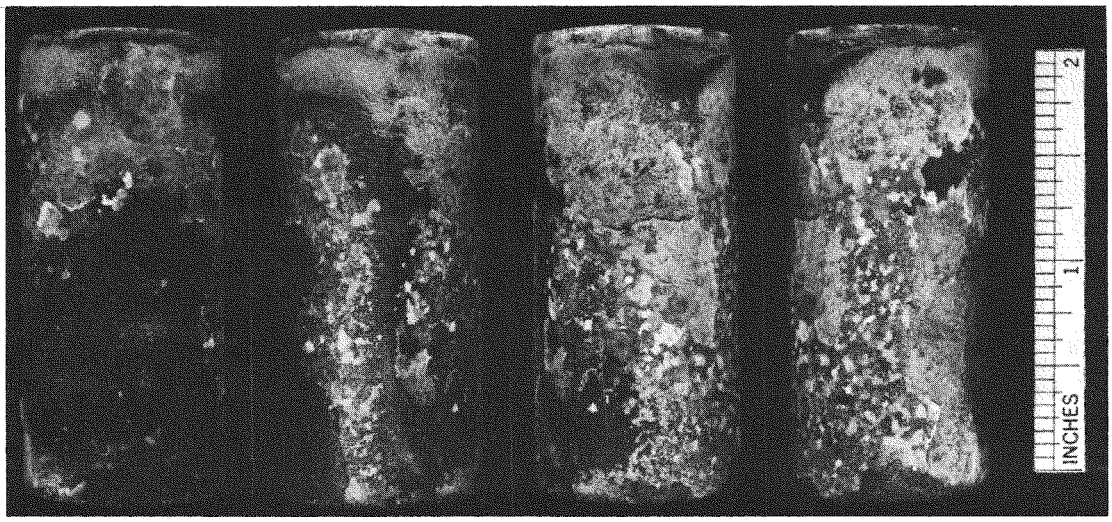

Figure 3-22 Four views of the NASA-coated specimen after 138 h of exposure at 1650°F maximum metal surface temperature with 5 ppm Na, 2 ppm V and 0.5 wt% S in the fuel.

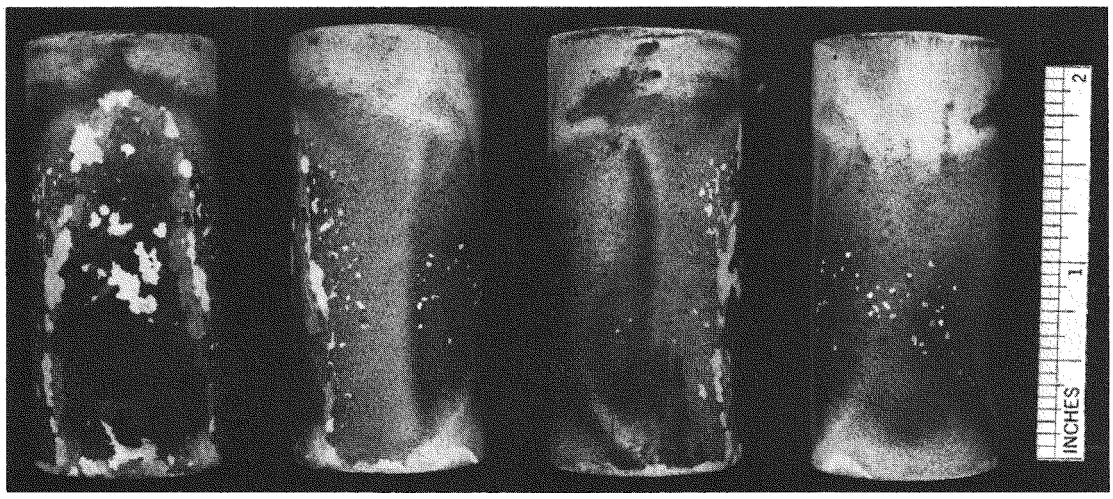

Figure 3-23 Four views of the Linde-coated specimen after 63.5 h of exposure at 1650°F maximum metal surface temperature with 5 ppm Na, 2 ppm V and 0.5 wt% S in the fuel.

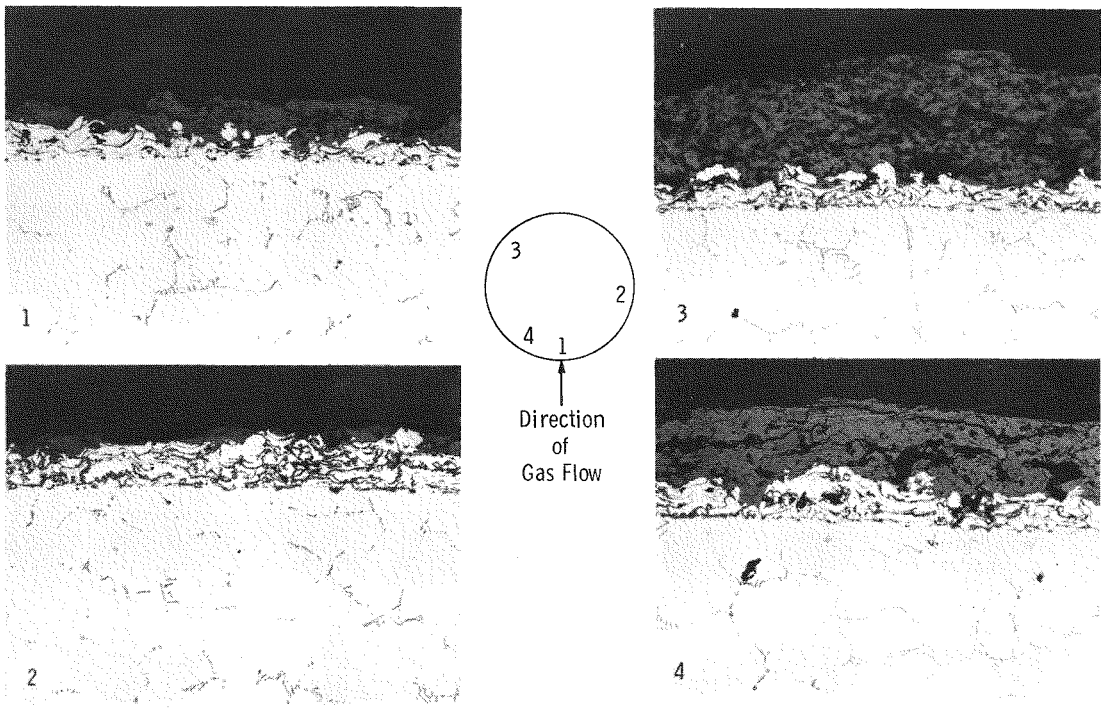

Figure 3-24 Metallographic cross-sections from four different regions of the NASA-coated specimen after 138 h of exposure at 1650°F maximum metal surface temperature with 5 ppm Na, 2 ppm V, and 0.5 wt% S in the fuel (100 X).

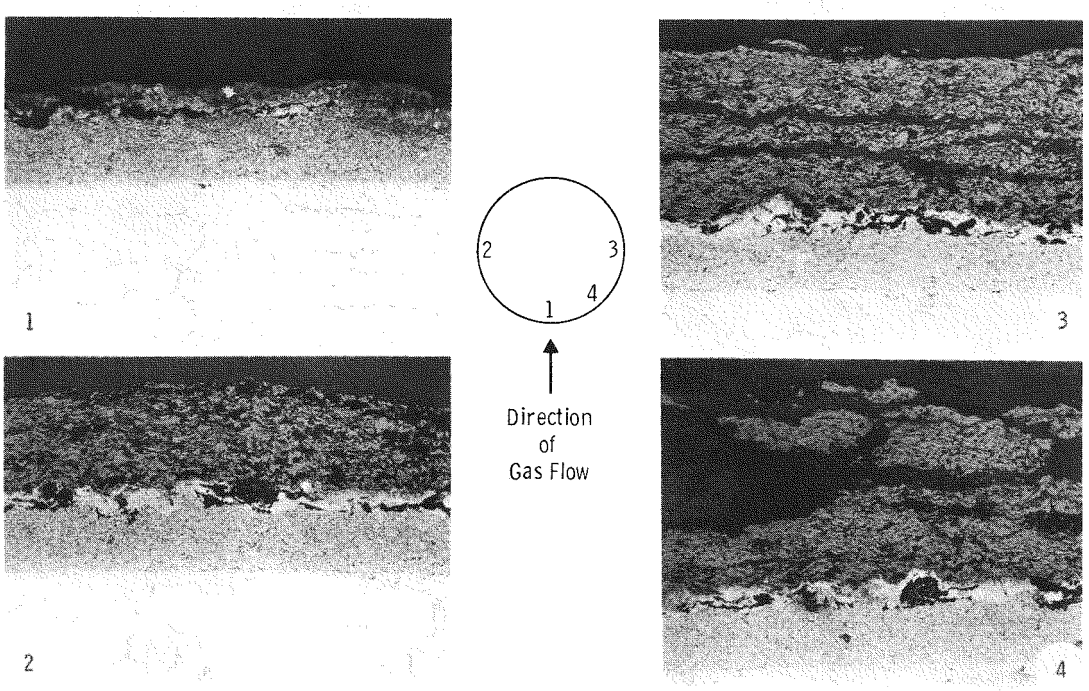

Figure 3-25 Metallographic cross-sections from four different regions of the Linde-coated specimen after 63.5 h of exposure at 1650°F maximum metal surface temperature with 5 ppm Na, 2 ppm V, and 0.5 wt% S in the fuel (100 X).

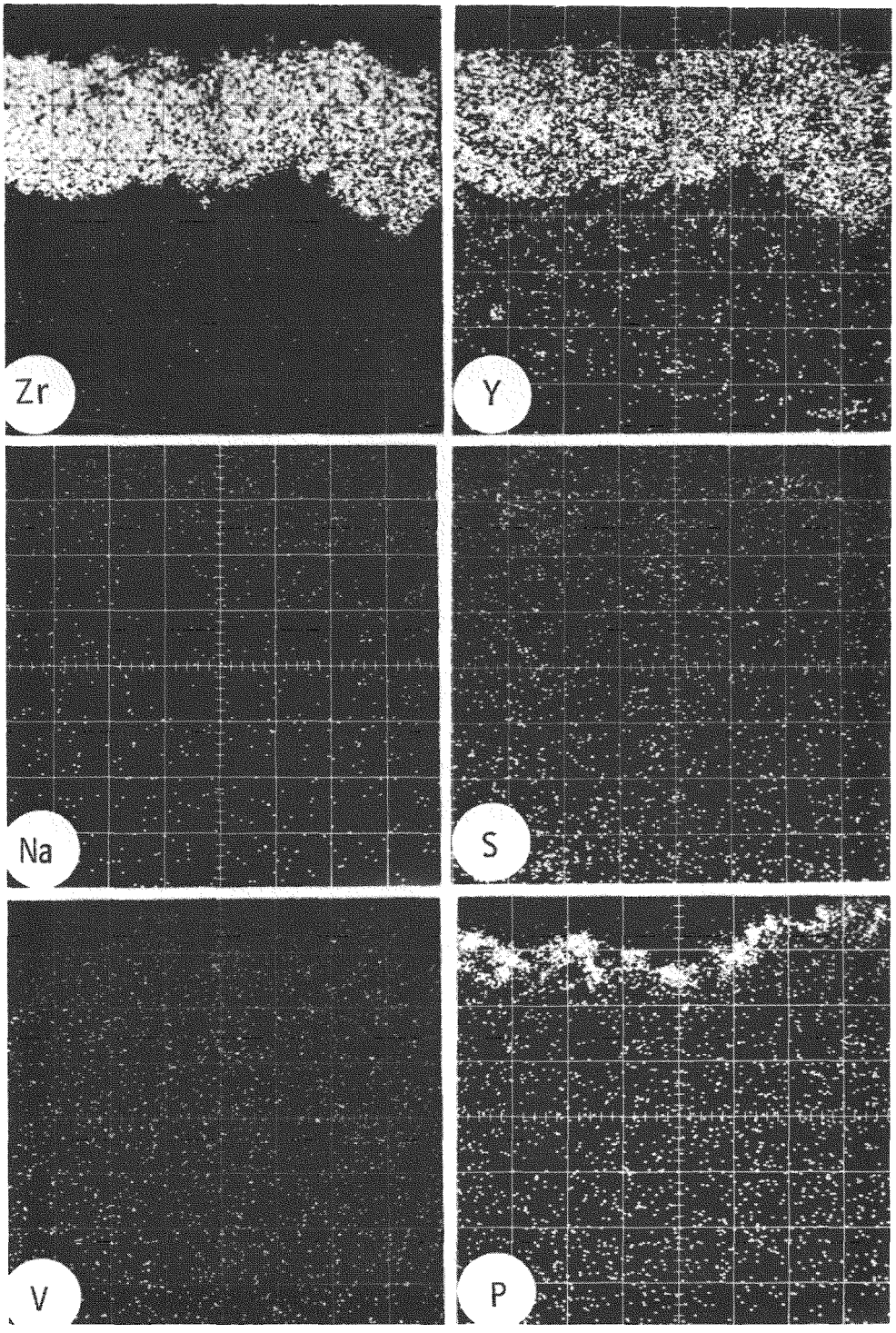

Figure 3-26 Electron microprobe scans from the Linde-coated specimen after 63.5 h of exposure at 1650°F maximum metal surface temperature with 5 ppm Na, 2 ppm V and 0.5 wt% S in the fuel (100 X).

develop in the oxide coating during exposure to the hot combustion gases which, in turn, cause spalling of the oxide coating. Again, no corrosion of the bond coat is apparent in these micrographs.

The electron microprobe scans for Zr, Y, Na, S, V and P from the surface of an exposed Linde-coated specimen from the above test are illustrated in Figure 3-26, which reveals that a significant amount of phosphorous gets concentrated in the $ZrO_2(Y_2O_3)$ overcoat in addition to minor amounts of Na, S, and V. X-ray diffraction analysis identified the following phases in the surface of the exposed specimens: $ZrO_2(Y_2O_3)$ (tetragonal/cubic)(major), ZrO_2 (monoclinic)(minor), $NaZr_2(PO_4)_3$ (minor), YPO_4 (minor), Na_2SO_4 (traces), α-Fe_2O_3 (trace) and spinel (trace). Thus, it is apparent that some yttrium in the oxide coating reacts with phosphorous from the combustion gases, and some tetragonal/cubic ZrO_2 is transformed to the monoclinic phase. Spinel and α-Fe_2O_3 evidently come from the stainless steel structural parts in the pressurized turbine test passage.

PARAMETRIC TESTS - COOLED TEST SPECIMENS

In order to separate the effects of various fuel contaminants on oxide coating cracking and spalling, a series of six parameter tests were conducted in the pressurized turbine test passage using GT-2 diesel oil (Exxon 260) as the basic fuel to which different contaminants were added. These tests were conducted at 2000°F gas temperature, keeping the maximum metal surface temperature at ∿1500°F. This means an average metal surface temperature of ∿1250°F. The typical temperatures experienced by different regions of the metal surface in these tests are illustrated in Figure 3-27.

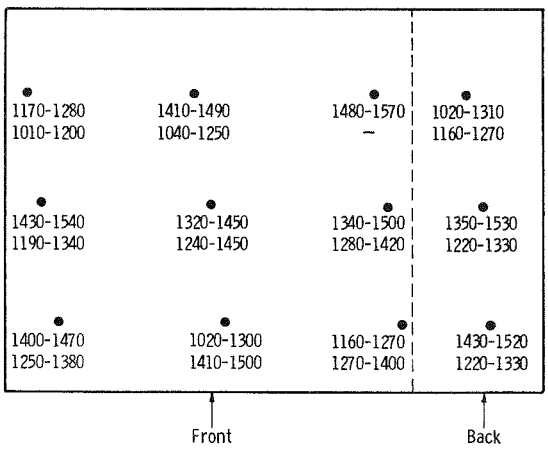

Figure 3-27 Typical temperatures (in °F) at the metal surface of the air-cooled specimens in the pressurized turbine test passage at 2000°F gas temperature, for the parametric tests.

The different fuel conditions under which this series of tests were conducted, the test duration, and the condition of the coating after test are summarized in Table 3-2. One NASA-coated and one Linde-coated specimen was exposed to each of these tests. Results from these tests are described below.

Table 3-2

SUMMARY OF PARAMETRIC TESTS WITH COOLED SPECIMENS

Test No.	Fuel Dopant[a]	Total Test Time	Coating Condition After Test
1	None	98 h	Coating intact
2	1 ppm Na	131 h	Coating intact
3	10 ppm V	42 h	Coating chipped and spalled
4	10 ppm V KI-16 Mg additive[b]	52 h	Coating chipped and spalled
5	1 ppm Na, 10 ppm V, 0.5 wt% S (W) Cr-Mg-Si additive[c]	59 h	Coating chipped and spalled
6	10 ppm V (W) Cr-Mg-Si additive[c]	41 h	Coating chipped and spalled

[a]Basic Fuel: GT-2 diesel oil (Exxon 260).

[b]Manufactured by Tretolite Division, Petrolite Corporation, St. Louis, MO.

[c]Westinghouse proprietary additive

Test No. 1 (Clean Fuel with No Dopants)

In this test, the coating remained intact and free of any macrocracking or spalling in 98 h of exposure to combustion gases. This is apparent in the photographs (four views of each specimen) of the surface of the exposed specimens shown in Figures 3-28 and 3-29. The surface did pick up small amounts of deposits from the combustion gases. The micrographs of the exposed NASA- and Linde-coated specimens from four different regions around the circumference of each specimen are shown in Figures 3-30 and 3-31, respectively. The oxide coating on the Linde-coated specimen shows some longitudinal cracking even though the coating did remain intact. Long-term exposure is requried to assess the effect of such microcracking on coating integrity.

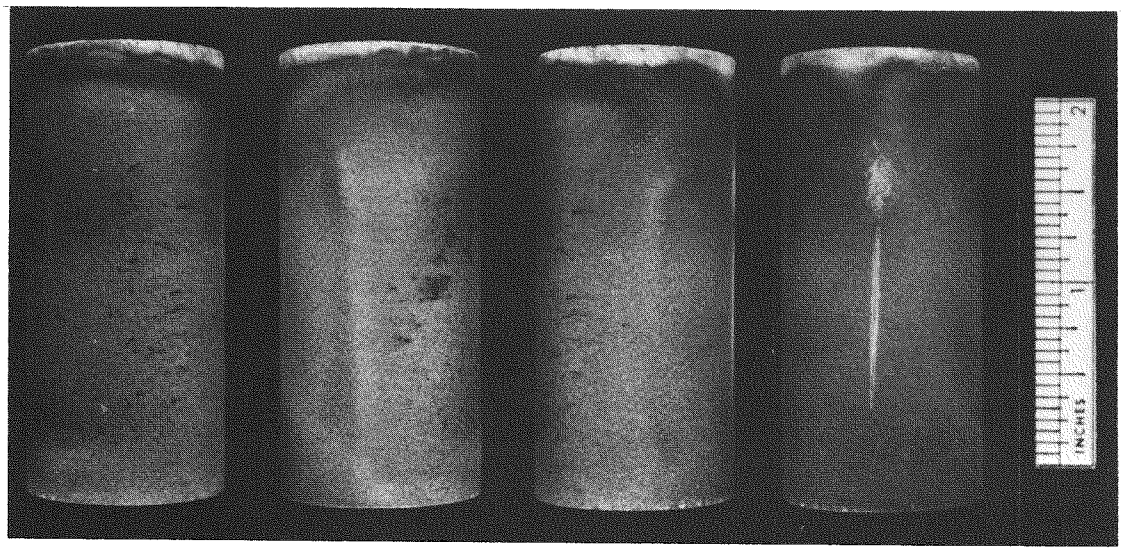

Figure 3-28 Four views of the NASA-coated specimen after 98 h of exposure in the clean fuel.

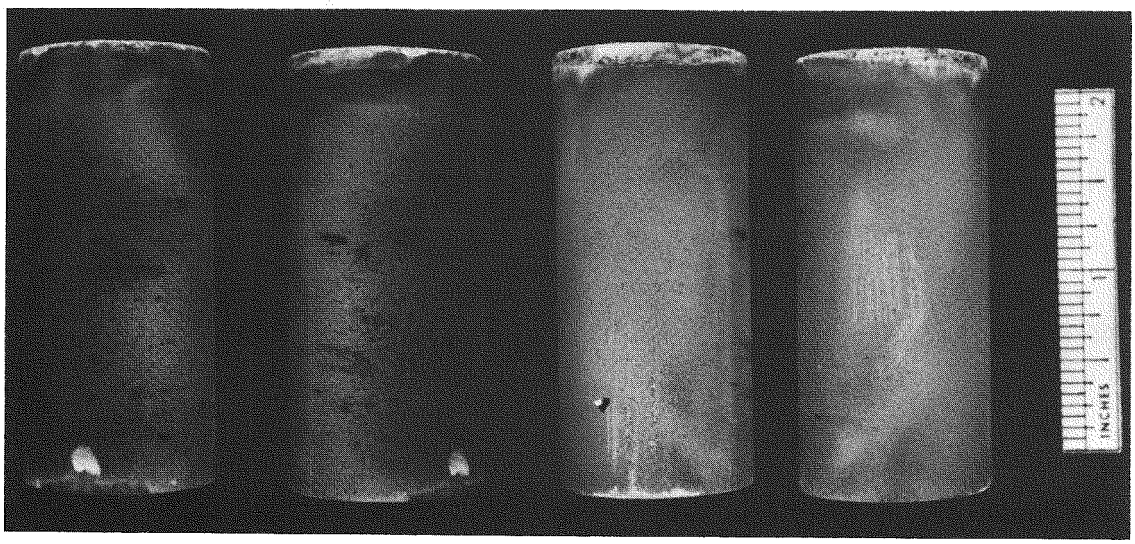

Figure 3-29 Four views of the Linde-coated specimen after 98 h of exposure in the clean fuel.

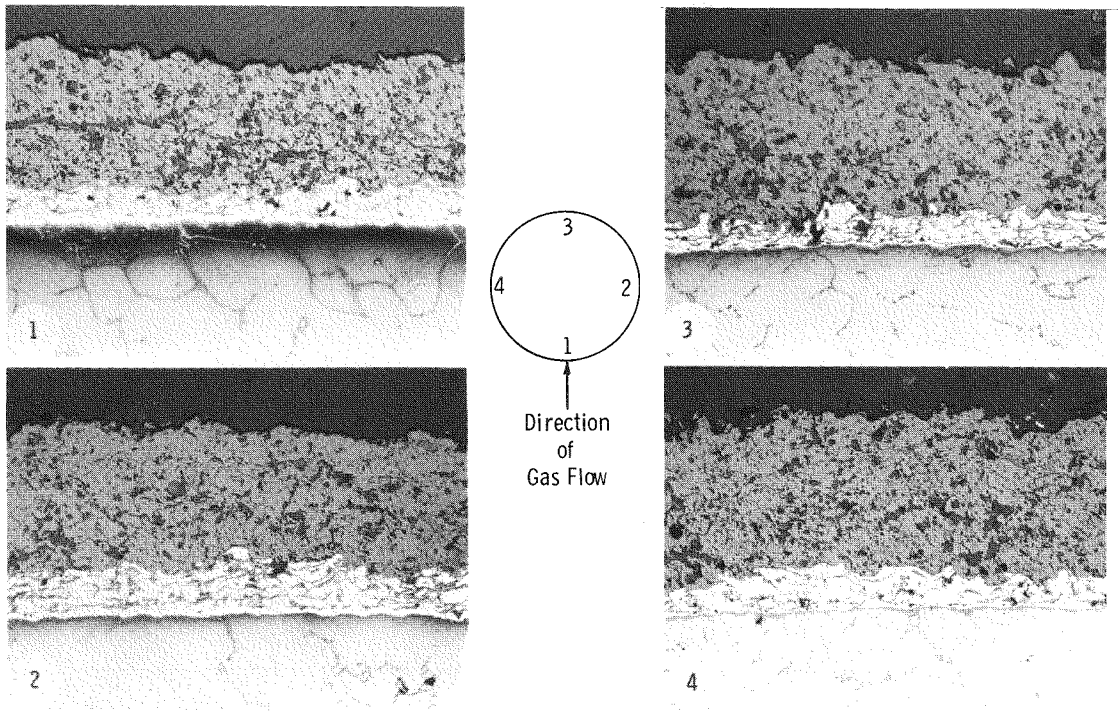

Figure 3-30 Metallographic cross-sections from four different regions of the NASA-coated specimen after 98 h of exposure in the clean fuel (100 X).

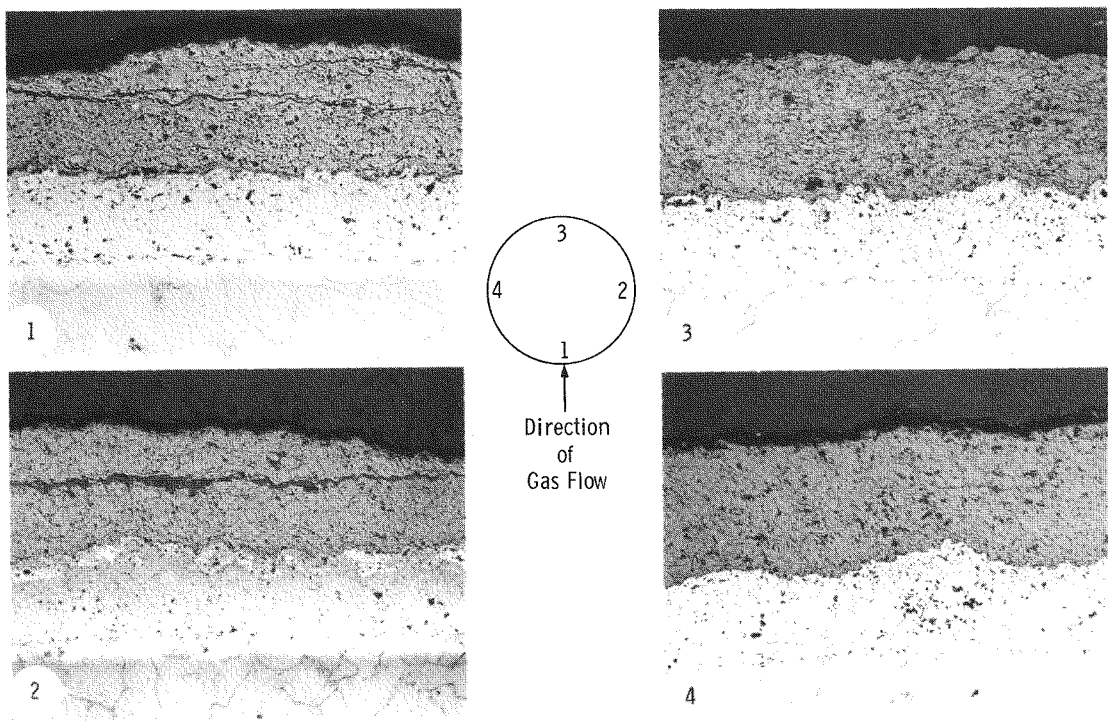

Figure 3-31 Metallographic cross-sections from four different regions of the Linde-coated specimen after 98 h of exposure in the clean fuel (100 X).

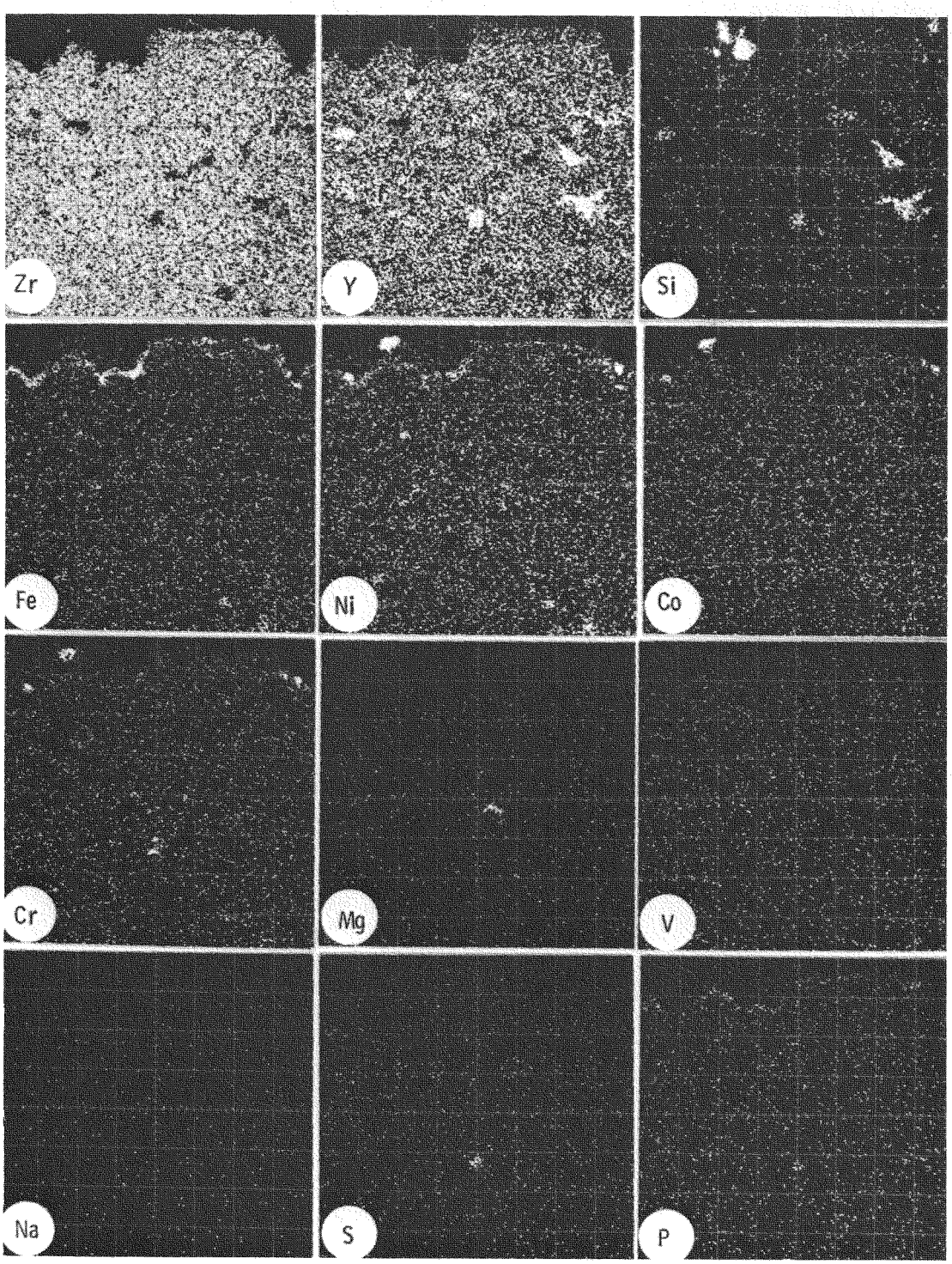

Figure 3-32 Electron microprobe scans from the NASA-coated specimen after 98 h of exposure in the clean fuel.

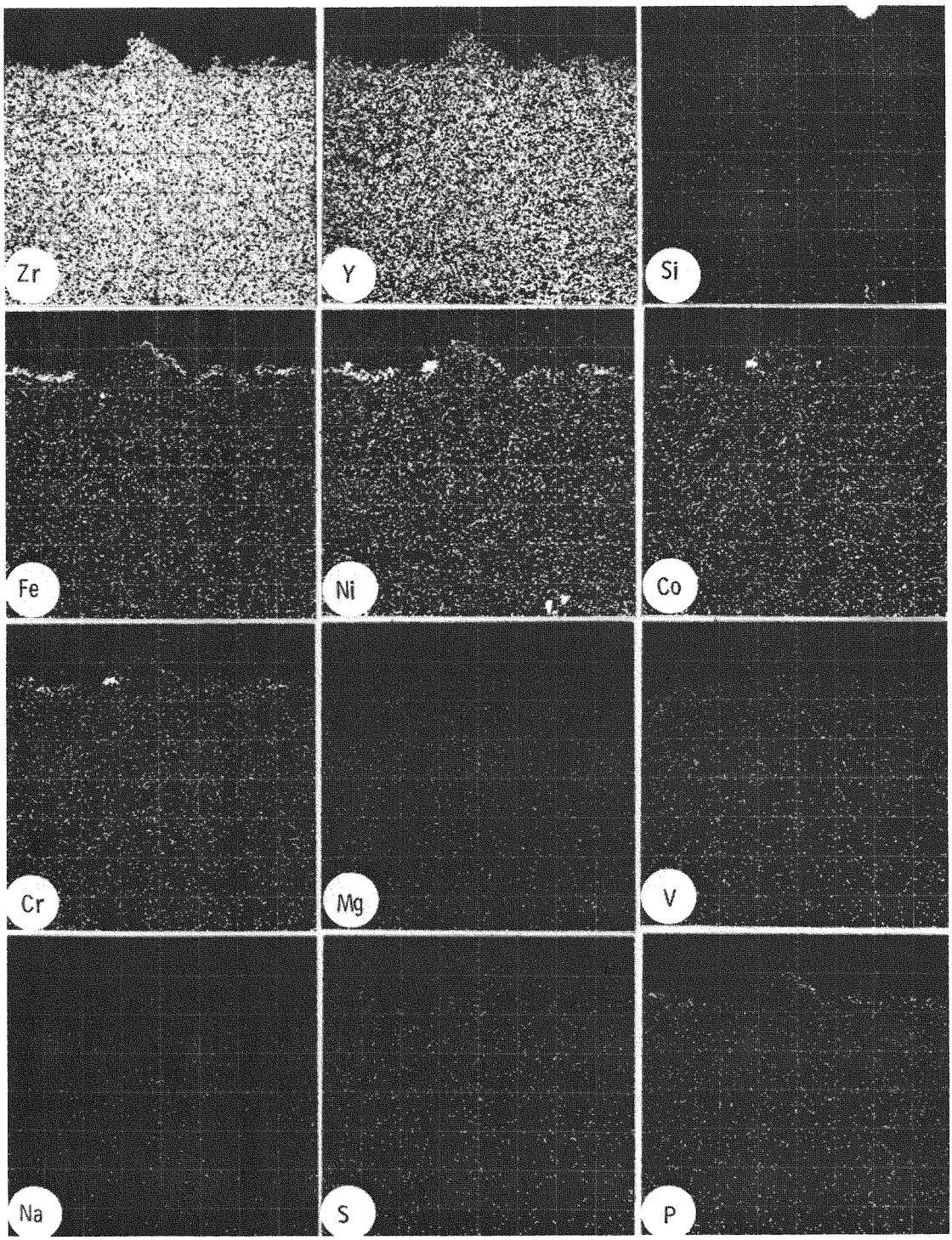

Figure 3-33 Electron microprobe scans from the Linde-coated specimen after 98 h of exposure in the clean fuel.

The electron microprobe scans from the exposed NASA- and Linde-coated specimens are shown in Figures 3-32 and 3-33, respectively. These scans show appreciable amounts of Fe, Ni, Co and Cr on the surface of the $ZrO_2(Y_2O_3)$ oxide coating. These elements are from the surface deposits of α-Fe_2O_3 and spinel, which come from the metallic structural parts of the pressurized turbine test passage. Also evident in these scans is a trace amount of phosphorous at the oxide surface. Phosphorous is present in the basic clean fuel as shown in Table 3-1. In the scans from the NASA-coated specimen (Figure 3-32), the Y + Si regions in the oxide coating are also apparent. These Y + Si regions are present in the as-received unexposed NASA coatings.

X-ray diffraction analysis identified predominantly $ZrO_2(Y_2O_3)$ (tetragonal/cubic) in the surface oxide; however, minor amounts of spinel and α-Fe_2O_3, and trace amounts of ZrO_2 (monoclinic), YPO_4 and $NaZr_2(PO_4)_3$ were also detected.

Test No. 2 (With 1 ppm Na in the Fuel)

In this test also, the coating remained intact and free of any macrocracking or spalling even after 131 h of exposure to combustion gases. This is clear from the photographs of the surface of the exposed NASA- and Linde-coated specimens shown in Figures 3-34 and 3-35, respectively. However, the micrographs of the exposed specimens, Figures 3-36 and 3-37, indicate considerable longitudinal cracking in the oxide overcoat, both for the NASA- and the Linde-coated specimens. Again, long-term exposure is required to assess the effect of this cracking on coating integrity.

The electron microprobe scans from the exposed NASA- and Linde-coated specimens are shown in Figures 3-38 and 3-39, respectively. Similar to that found in Test No. 1 in the clean fuel, these scans show considerable amounts of Fe-, Ni-, Co- and Cr-containing deposits on the oxide surface. X-ray diffraction analysis identified $ZrO_2(Y_2O_3)$ (tetragonal/cubic) as the major phase in the oxide surface with minor amounts of spinel, α-Fe_2O_3 and ZrO_2 (monoclinic), and traces of YPO_4.

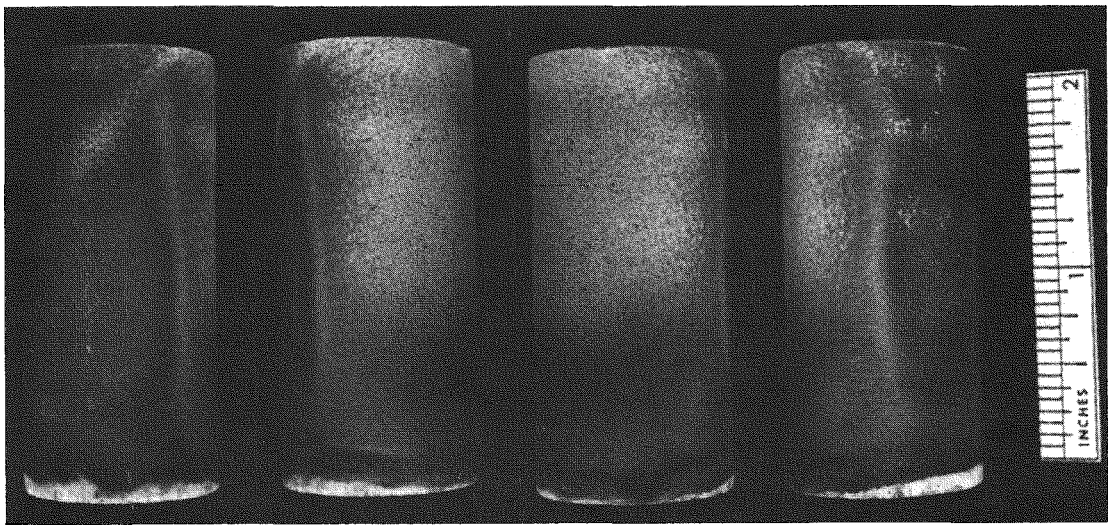

Figure 3-34 Four views of the NASA-coated specimen after 131 h of exposure with 1 ppm Na in the fuel.

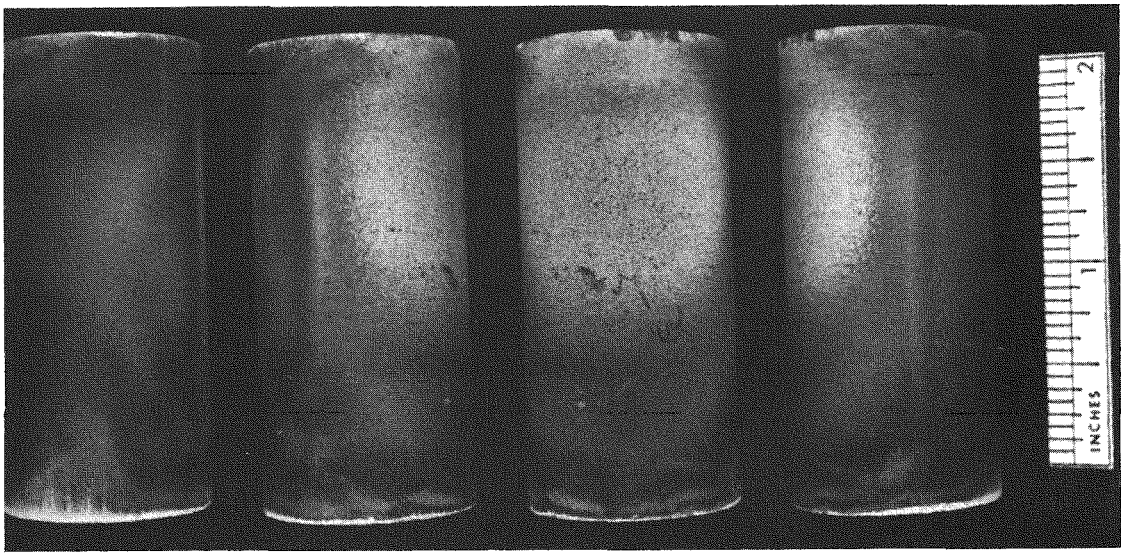

Figure 3-35 Four views of the Linde-coated specimen after 131 h of exposure with 1 ppm Na in the fuel.

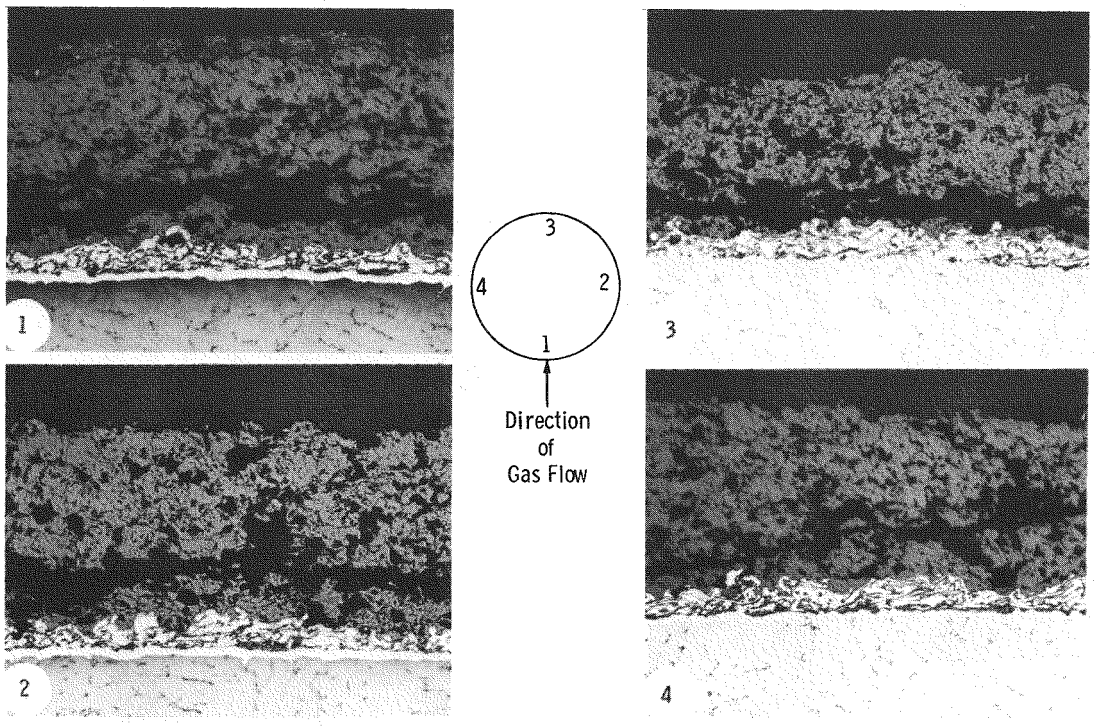

Figure 3-36 Metallographic cross-sections from four different regions of the NASA-coated specimen after 131 h of exposure with 1 ppm Na in the fuel (100 X).

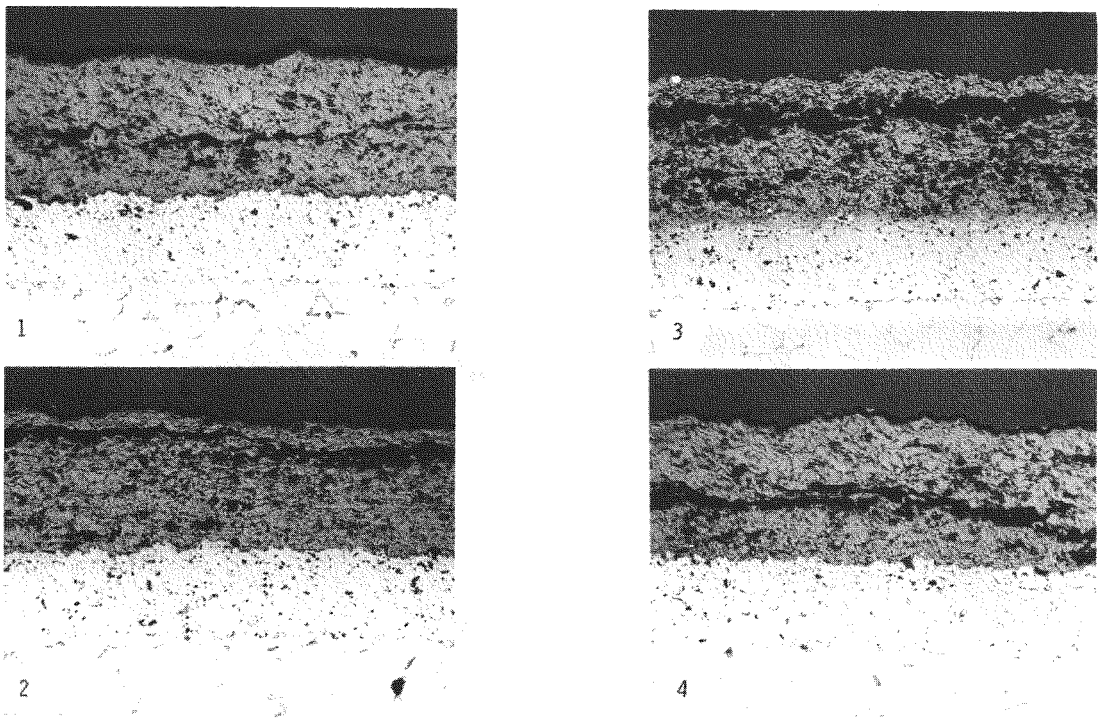

Figure 3-37 Metallographic cross-sections from four different regions of the Linde-coated specimen after 131 h of exposure with 1 ppm Na in the fuel (100 X).

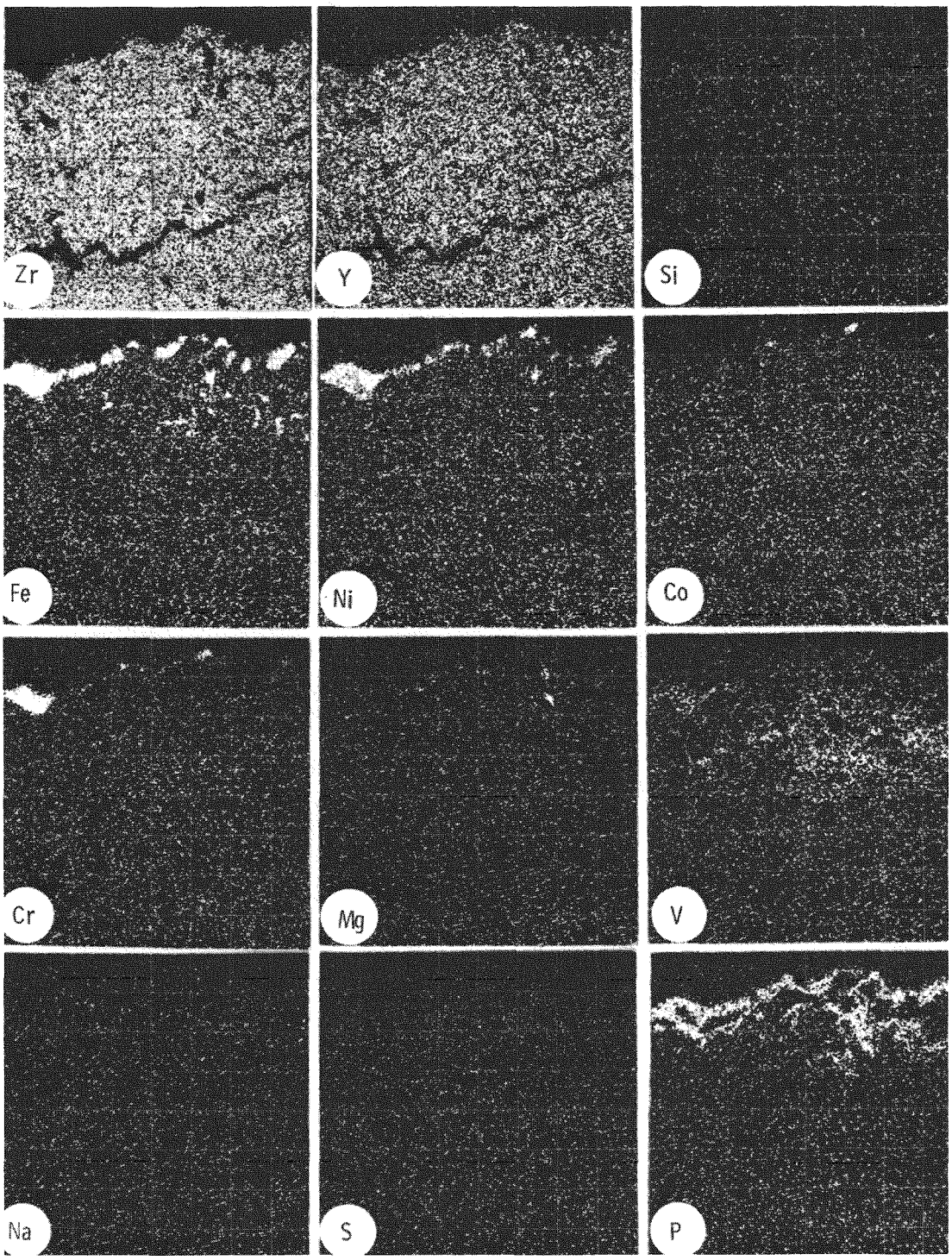

Figure 3-38 Electron Microprobe scans from the NASA-coated specimen after 131 h of exposure with 1 ppm Na in the fuel.

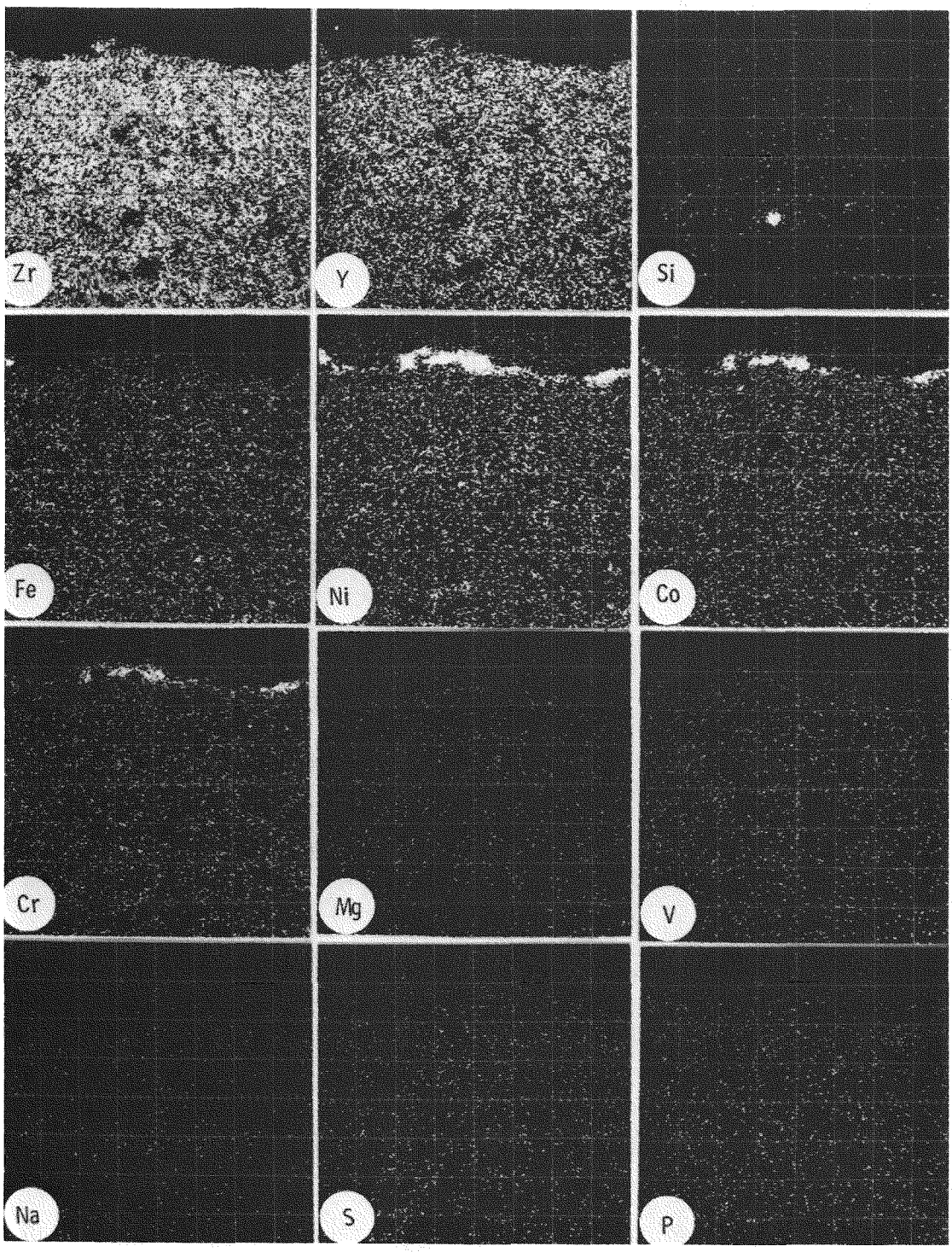

Figure 3-39 Electron microprobe scans from the Linde-coated specimen after 131 h of exposure with 1 ppm Na in the fuel.

Test No. 3 (With 10 ppm V in the Fuel)

In this test, the oxide coating chipped and spalled after only 42 h of exposure to combustion gases. The most chipping and spalling occurred on the front sides of the specimens which faced the gas flow. This is evident from the photographs of the exposed specimens, Figures 3-40 and 3-41, and the micrographs from four different regions of the exposed specimens shown in Figures 3-42 and 3-43. These micrographs indicate that the oxide coating cracks and spalls off from within its own thickness rather than at the MCrAlY/oxide interface.

The electron microprobe scans from the exposed NASA- and Linde-coated specimens are shown in Figures 3-44 and 3-45, respectively. These scans reveal that significant amounts of vanadium and phosphorous penetrate inside the oxide coating during exposure to the combustion gases. Also evident in the microprobe scans are surface deposits rich in Fe, Co, Ni and Cr which were found in all the experiments. X-ray diffraction analysis identified $ZrO_2(Y_2O_3)$ (tetragonal/cubic) as the predominant phase in the oxide coating with minor amounts of ZrO_2 (monoclinic), spinel, α-Fe_2O_3, YPO_4 and $NaZr_2(PO_4)_3$.

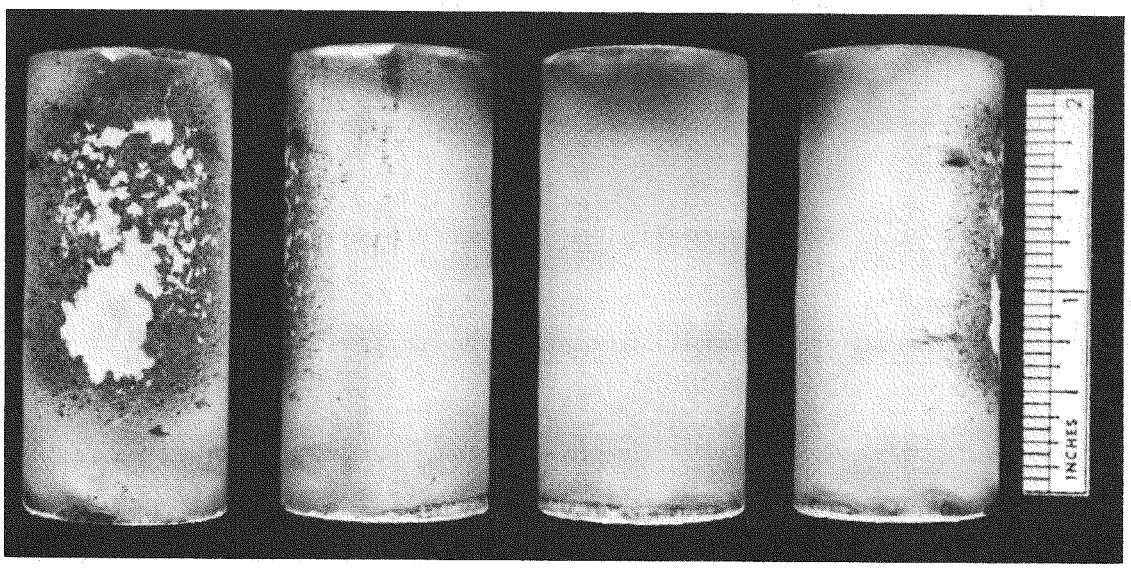

Figure 3-40 Four views of the NASA-coated specimen after 42 h of exposure with 10 ppm V in the fuel.

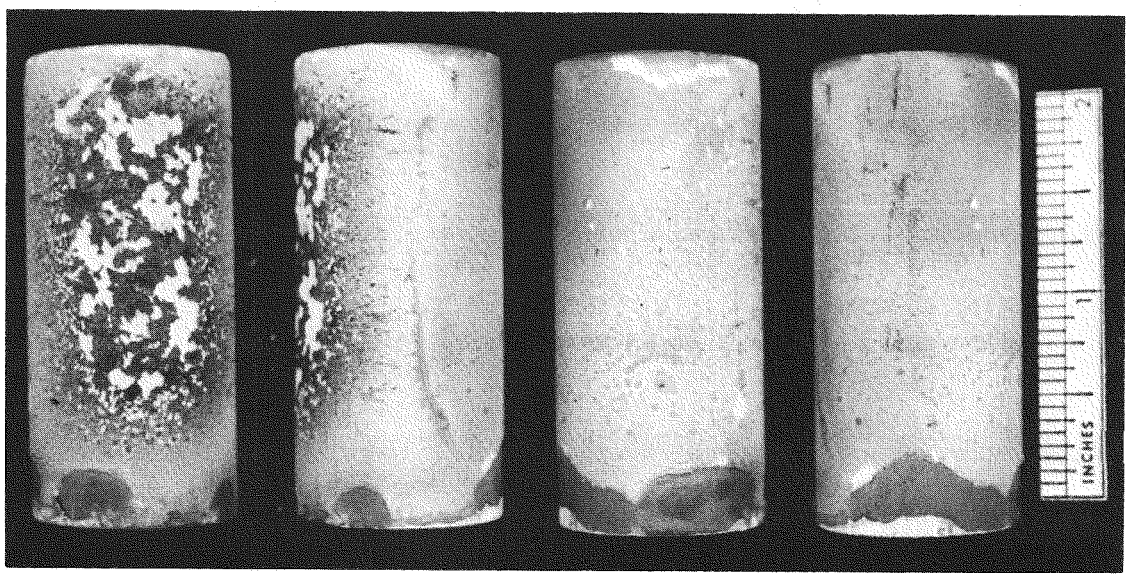

Figure 3-41 Four views of the Linde-coated specimen after 42 h of exposure with 10 ppm V in the fuel.

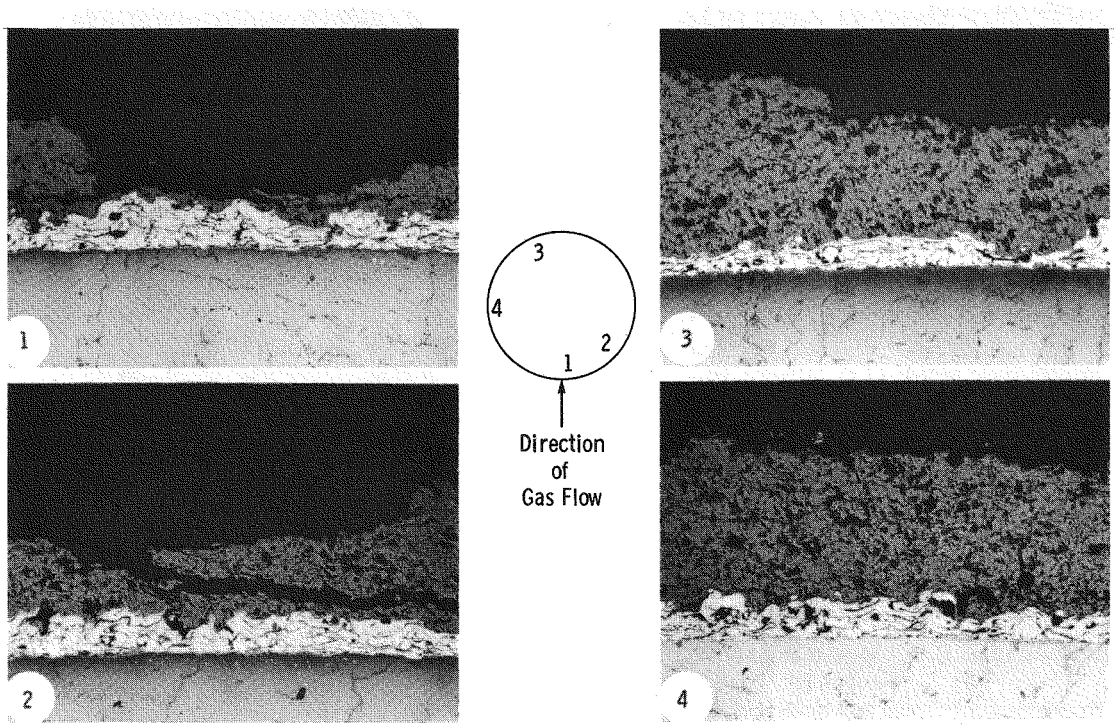

Figure 3-42 Metallographic cross-sections from four different regions of the NASA-coated specimen after 42 h of exposure with 10 ppm V in the fuel (100 X).

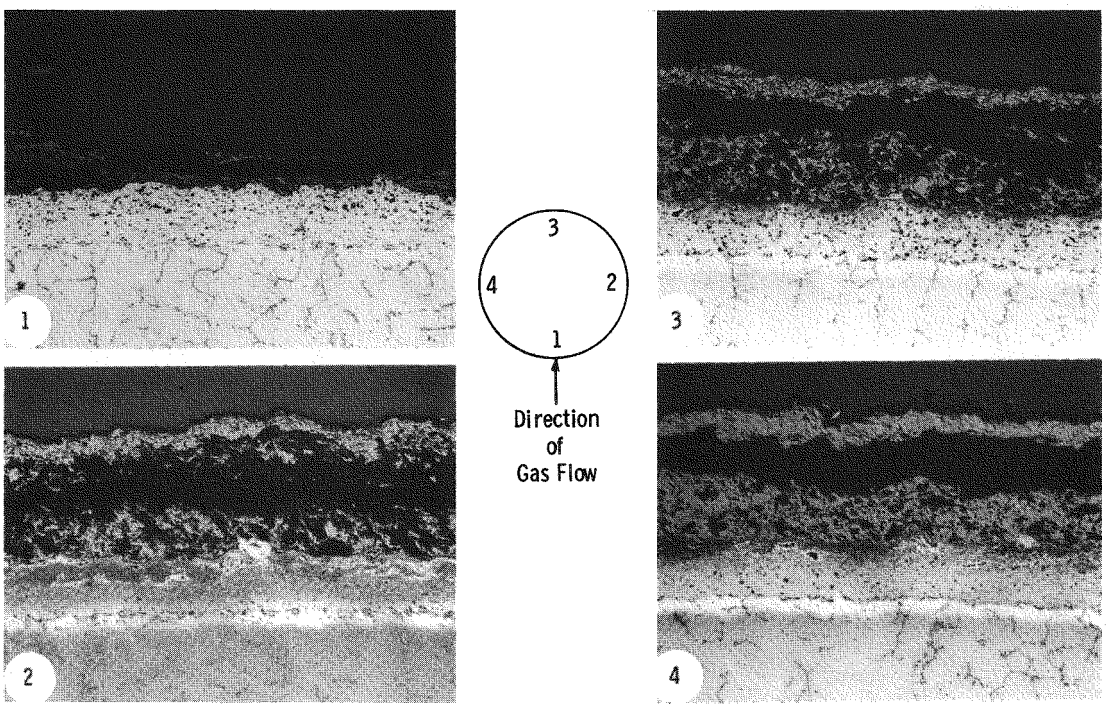

Figure 3-43 Metallographic cross-sections from four different regions of the Linde-coated specimen after 42 h of exposure with 10 ppm V in the fuel (100 X).

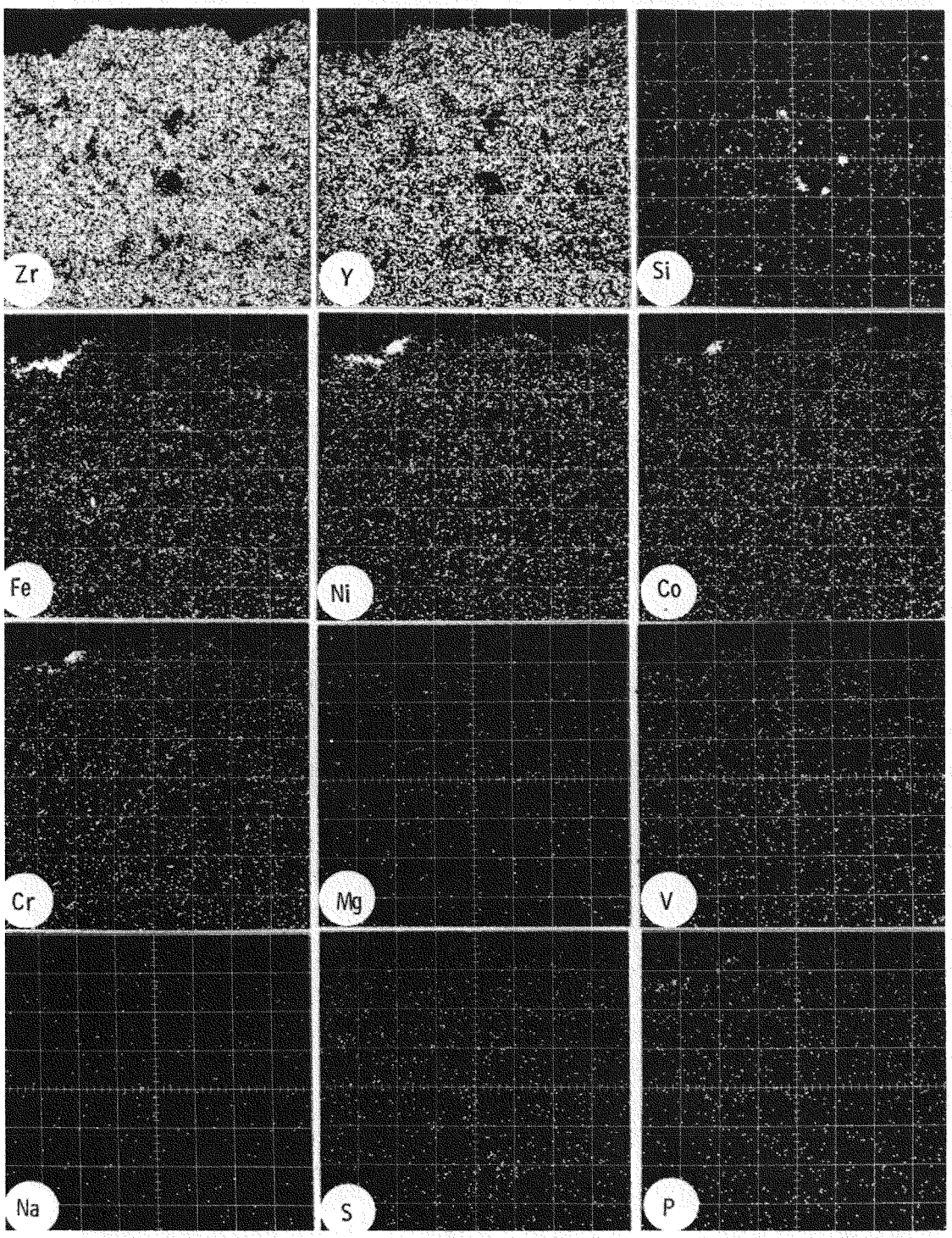

Figure 3-44 Electron microprobe scans from the NASA-coated specimen after 42 h of exposure with 10 ppm V in the fuel.

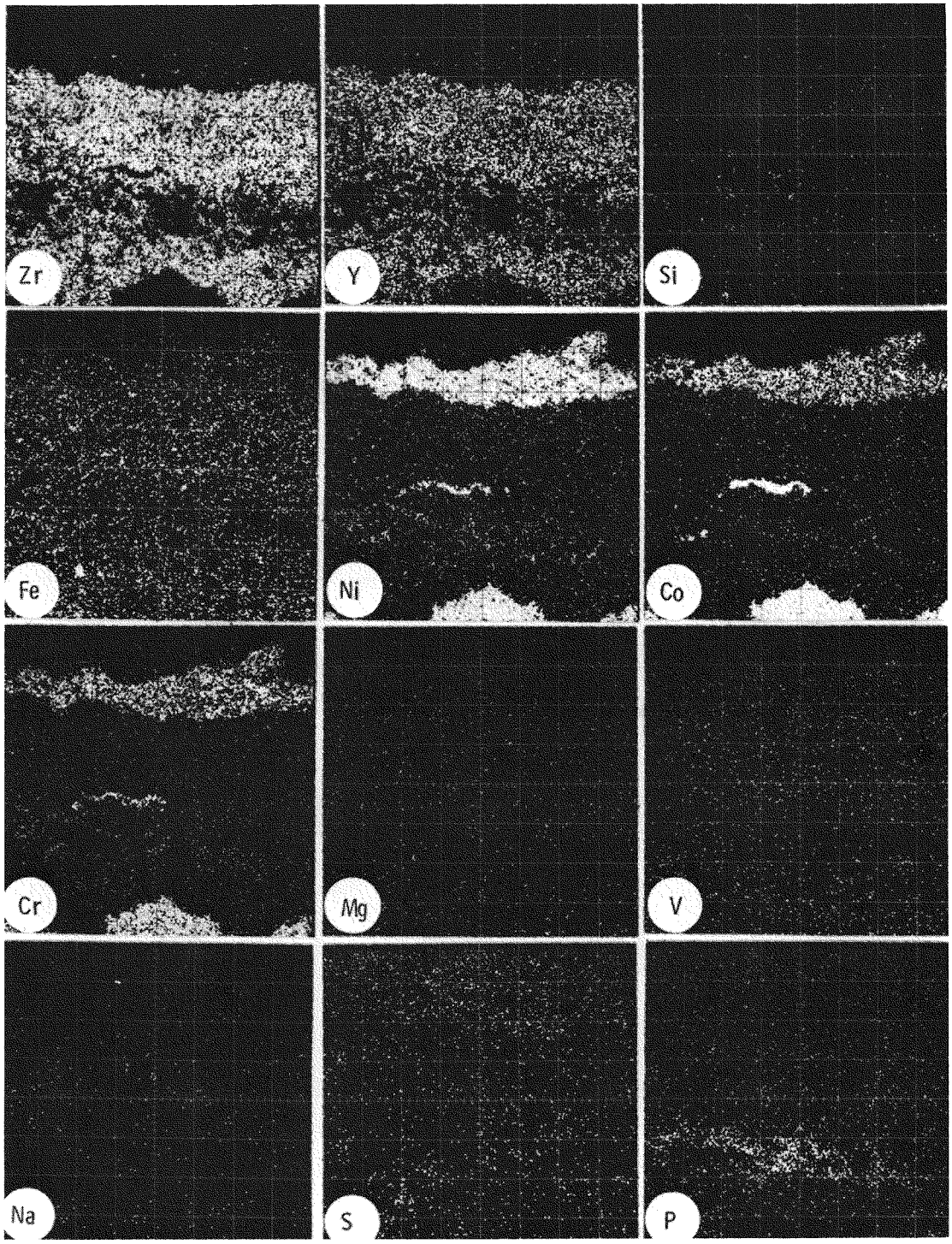

Figure 3-45 Electron microprobe scans from the Linde-coated specimen after 42 h of exposure with 10 ppm V in the fuel.

Test No. 4 (With 10 ppm V and Mg Additive)

In this test, a magnesium-based additive, KI-16 from Tretolite Division of the Petrolite Corporation, was added to the fuel in a quantity necessary to give Mg/V ratio equal to 3. However, this additive did not prove very successful, and the oxide coating again chipped and spalled off after as early as 26 h of exposure to combustion gases. The surface appearance of the exposed NASA- and Linde-coated specimens is shown in Figures 3-46 and 3-47, respectively, which show that the most attack occurred on the front of the specimen facing the gas flow. The micrographs of the exposed specimens. Figures 3-48 and 3-49, also indicate considerable cracking, chipping and spalling of the oxide coating.

The electron microprobe scans from the exposed NASA- and Linde-coated specimens, shown in Figures 3-50 and 3-51, indicate large concentrations of Mg, V and P on the surface of the oxide coating. Also apparent from these scans are Fe-, Co- and Cr-rich surface deposits. X-ray diffraction analysis detected $ZrO_2(Y_2O_3)$ (tetragonal/cubic), $Mg_3(PO_4)_2$, $Mg_3(VO_4)_2$, MgO, $MgSO_4$, $MgSO_4 \cdot 6H_2O$ and spinel in the surface coating. This magnesium in the KI-16 additive reacts with V and P in the fuel to form massive $Mg_3(VO_4)_2$ and $Mg_3(PO_4)_2$ deposits. However, the coating still cracks and spalls.

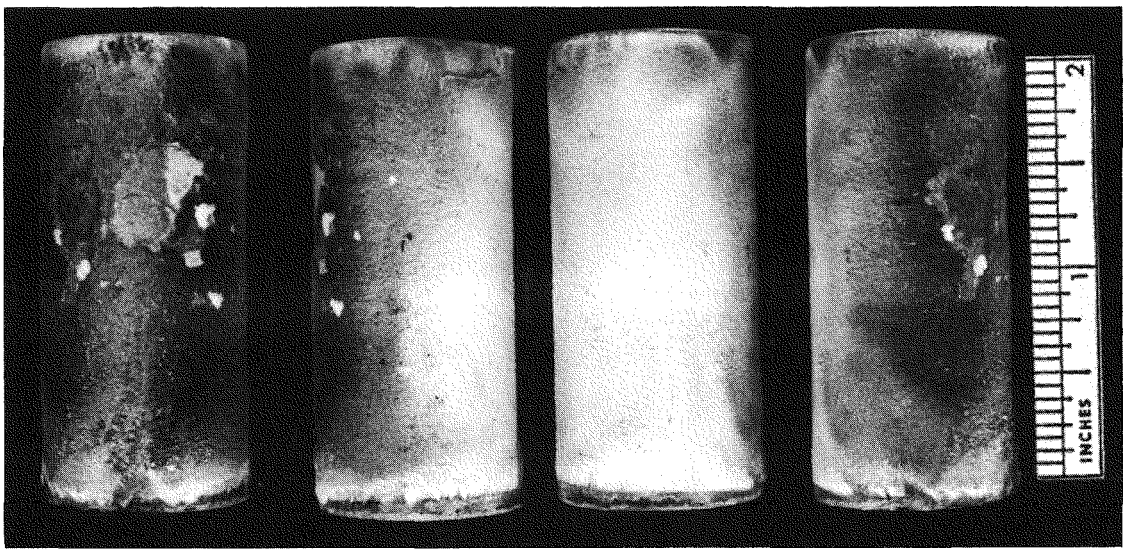

Figure 3-46 Front view of the NASA-coated specimen after 52 h of exposure with 10 ppm V and KI-16 magnesium-additive in the fuel.

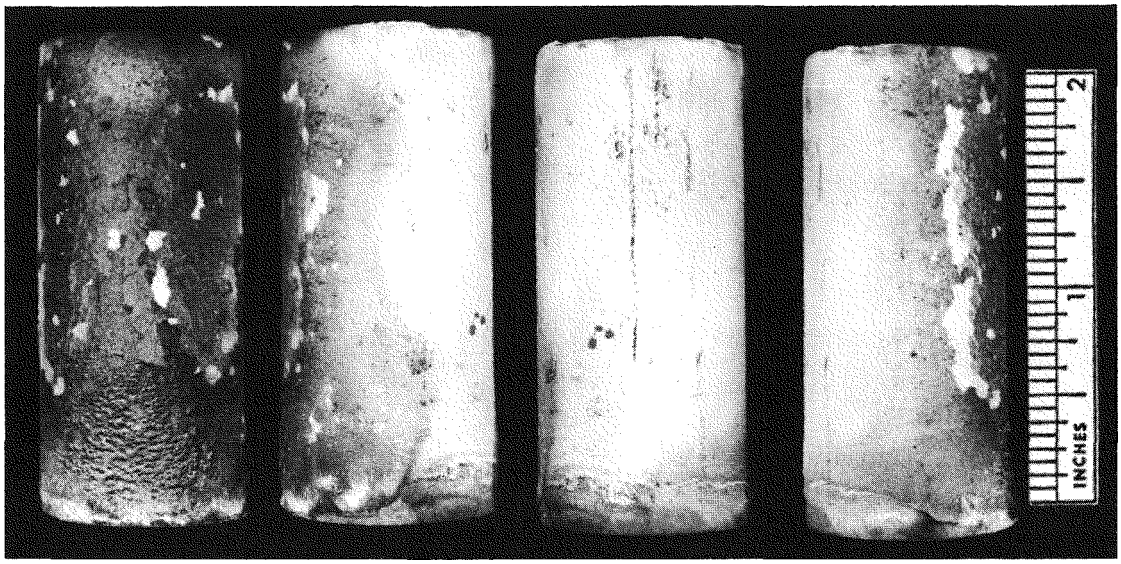

Figure 3-47 Four views of the Linde-coated specimen after 52 h of exposure with 10 ppm V and KI-16 magnesium-additive in the fuel.

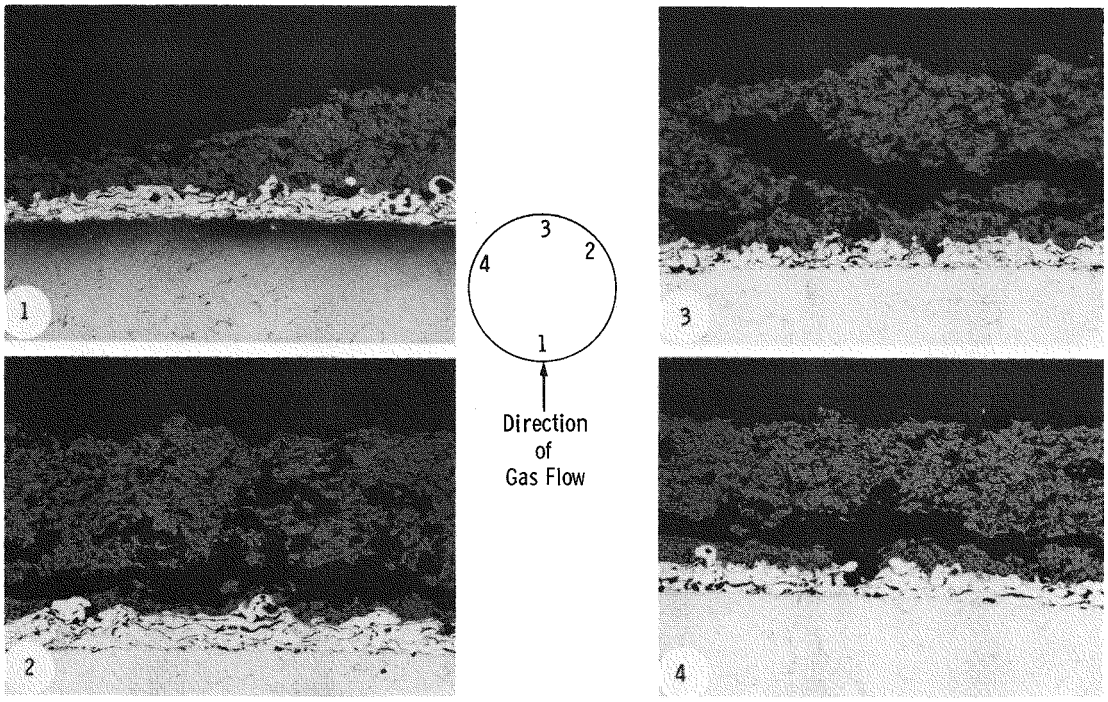

Figure 3-48 Metallographic cross-sections from four different regions of the NASA-coated specimen after 52 h of exposure with 10 ppm V and KI-16 magnesium additive in the fuel (100 X).

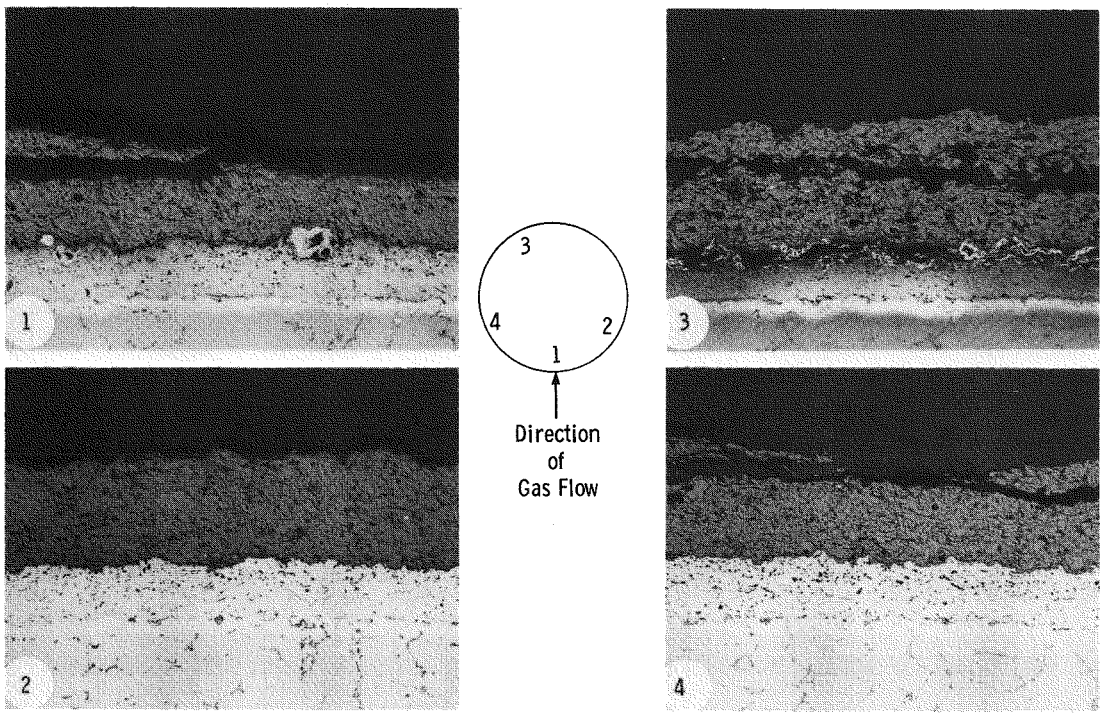

Figure 3-49 Metallographic cross-sections from four different regions of the Linde-coated specimen after 52 h or exposure with 10 ppm V and KI-16 magnesium additive in the fuel (100 X).

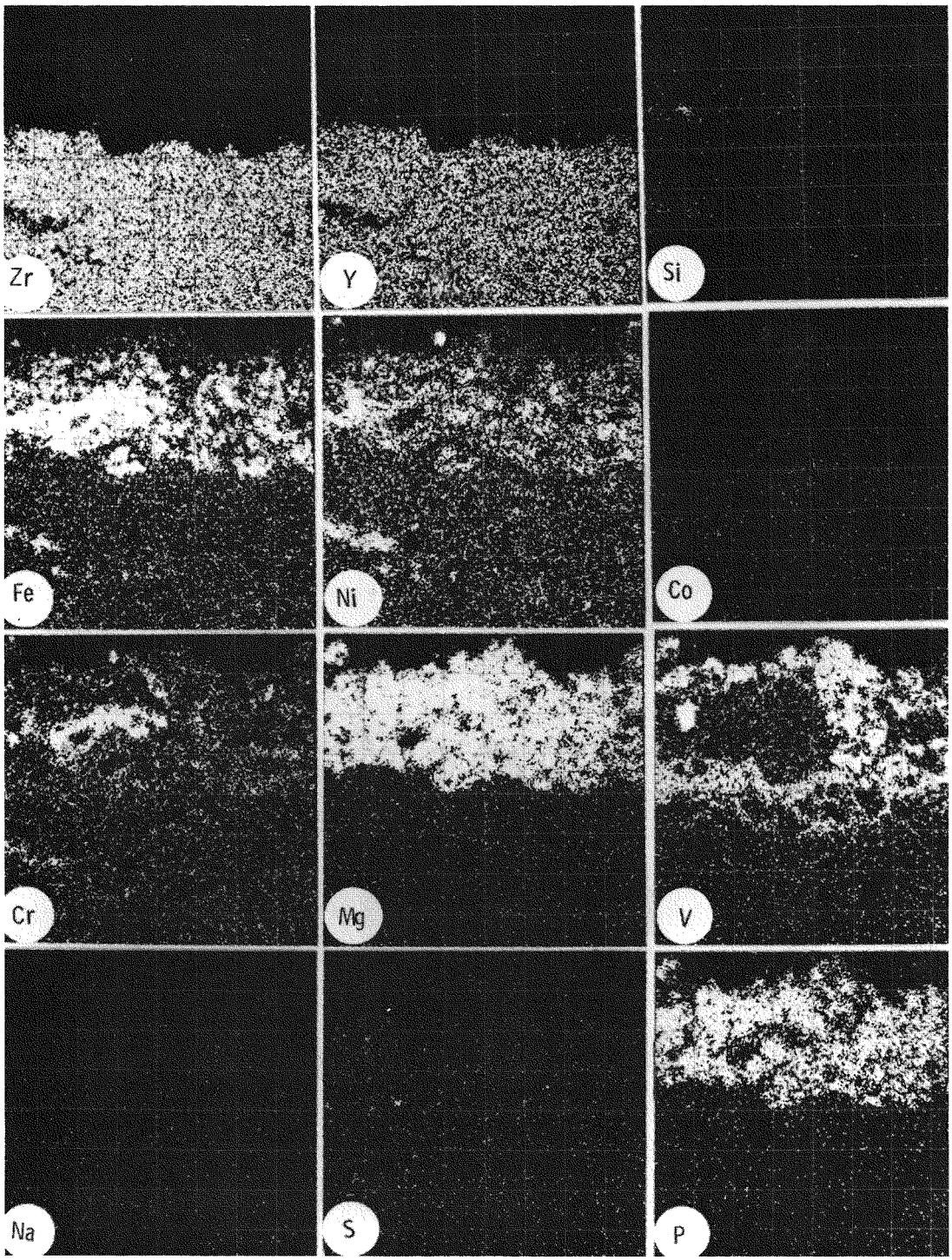

Figure 3-50 Electron microprobe scans from the NASA-coated specimen after 52 h of exposure with 10 ppm V and KI-16 magnesium additive in the fuel.

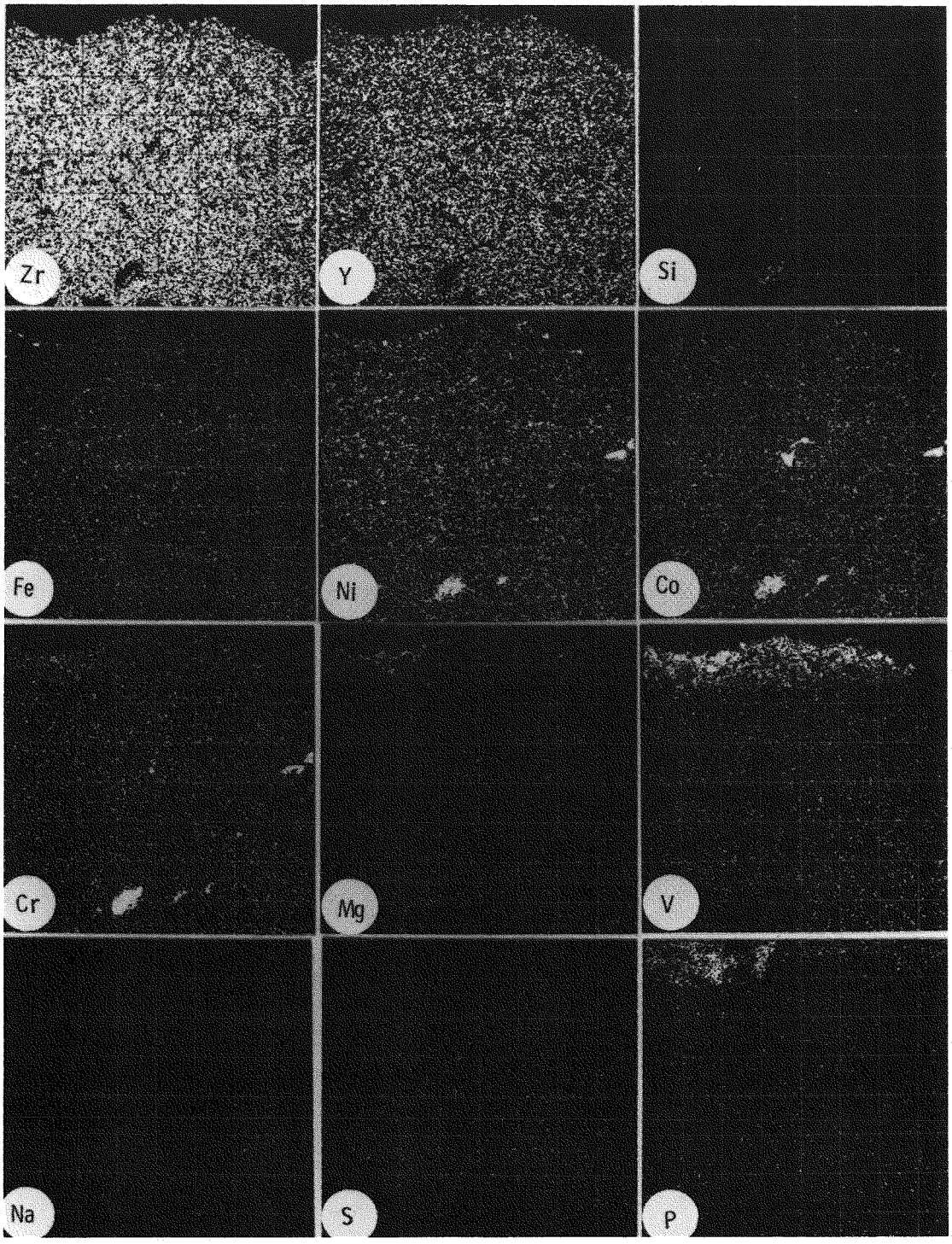

Figure 3-51 Electron microprobe scans from the Linde-coated specimen after 52 h of exposure with 10 ppm V and KI-16 magnesium additive in the fuel.

Test No. 5 (With 1 ppm Na, 10 ppm V, 0.5 wt% S and a Cr-Mg-Si Additive)

In this test, a proprietary Westinghouse additive, contianing Cr, Mg and Si, was added to the fuel with the objective or preventing corrosion by Na and V. However, even in the presence of this additive, the coating showed cracking and chipping in 59 h of exposure to combustion gases. This is clear from the photographs of the exposed NASA- and Linde-coated specimens shown in Figures 3-52 and 3-53, respectively. The cracking and chipping of the oxide coating is also evident in the micrographs of the exposed specimens shown in Figures 3-53 and 3-54.

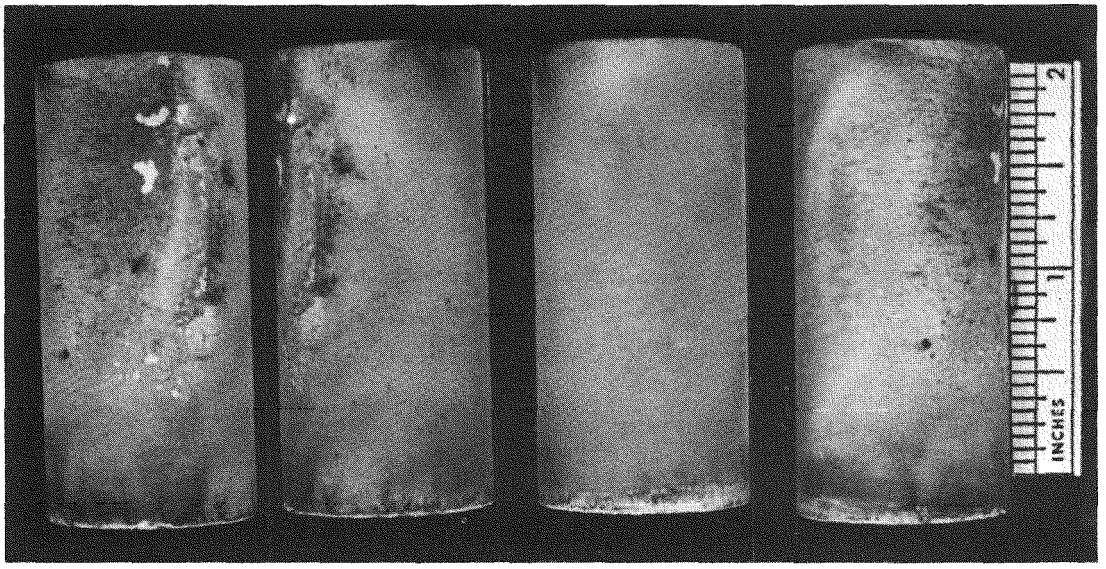

Figure 3-52 Four views of the NASA-coated specimen after 59 h of exposure with 1 ppm Na, 10 ppm V, o.5 wt% S and a Cr-Mg-Si additive in the fuel.

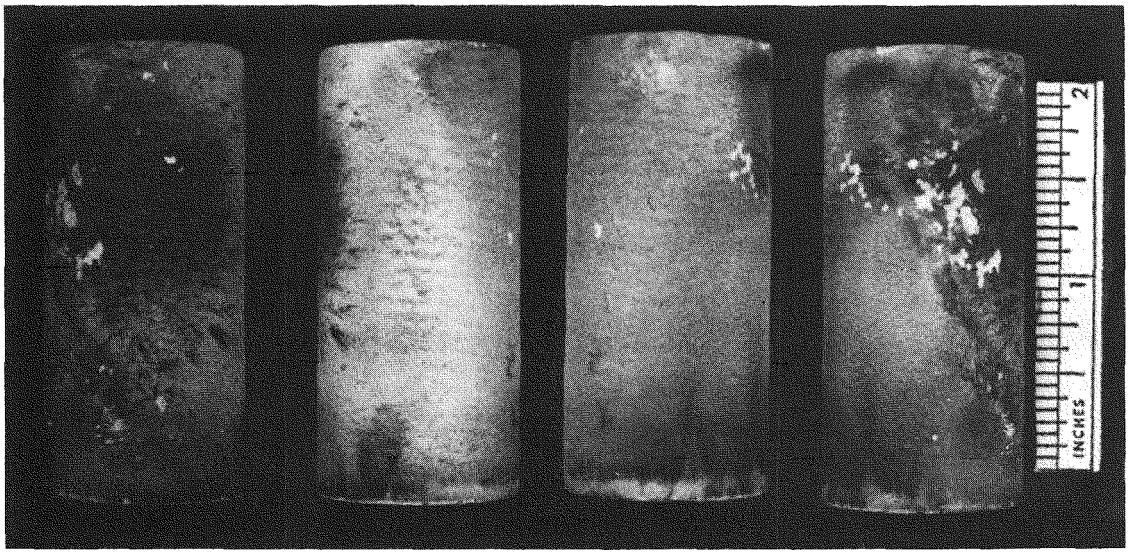

Figure 3-53 Four views of the Linde-coated specimen after 59 h of exposure with 1 ppm Na, 10 ppm V, 0.5 wt% S and a Cr-Mg-Si additive in the fuel.

X-ray diffraction analysis identified mainly $ZrO_2(Y_2O_3)$ (tetragonal/cubic), SiO_2 (quartz), SiO_2 (cristobalite), $Mg_3(PO_4)_2$, α-Fe_2O_3 and spinel in the surface coating. However, trace amounts of ZrO_2 (monoclinic) and $NaZr_2(PO_4)_3$ were also detected. Silica is apparently formed by oxidation of Si in the additive. Surprisingly, no magnesium vanadate or any other vanadium compound was detected in the surface after exposure to the combustion gases even though the additive was used in quantity sufficient to give a Mg/V ratio equal to 3, same as in Test No. 4. Apparently, either all the magnesium in the additive combined with phosphorous in the combustion gases to form $Mg_3(PO_4)_2$; or alternatively, if present, was not detected by X-ray diffraction analysis because the strongest diffraction line for $Mg_3(VO_4)_2$ coincides with the strongest diffraction line for $ZrO_2(Y_2O_3)$.

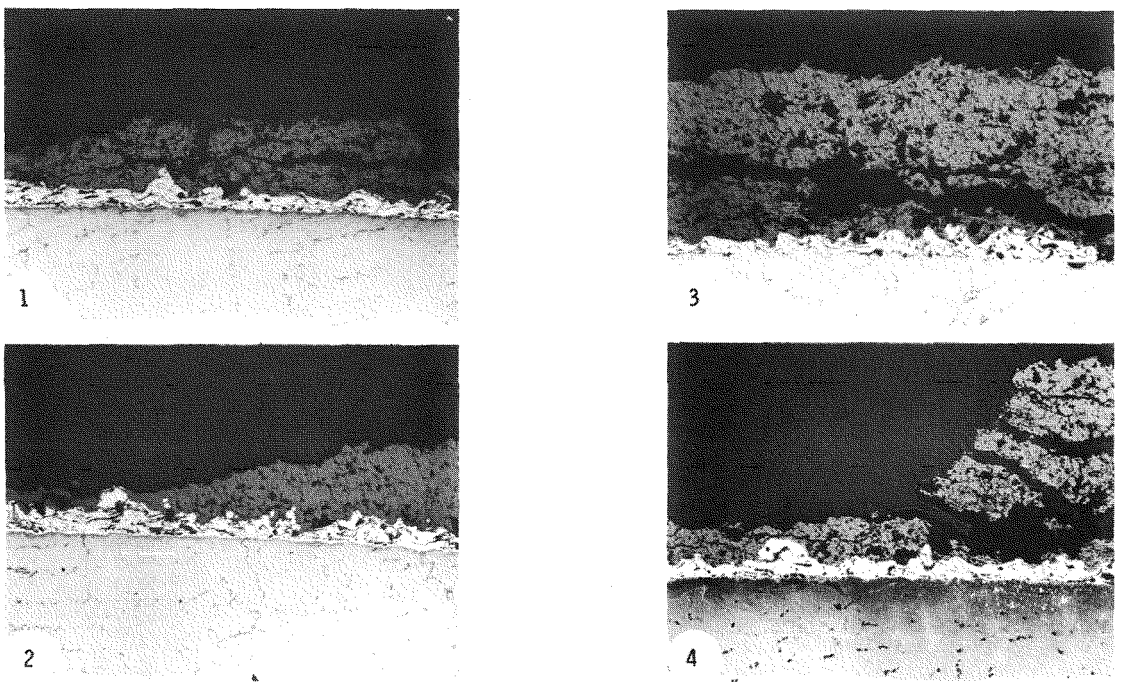

Figure 3-54 Metallographic cross-sections from four different regions of the NASA-coated specimen after 59 h of exposure with 1 ppm Na, 10 ppm V, 0.5 wt% S and a Cr-Mg-Si additive in the fuel (100 X).

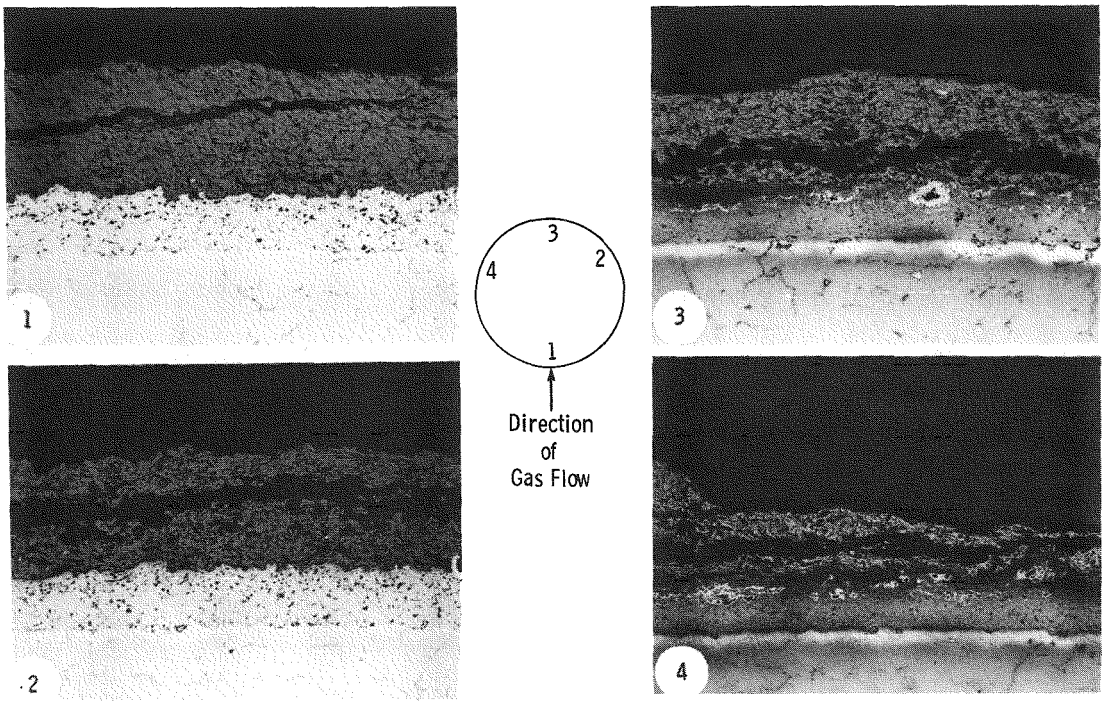

Figure 3-55 Metallographic cross-section from four different regions of the Linde-coated specimen after 59 h of exposure with 1 ppm Na, 10 ppm V, and 0.5 wt% S and a Cr-Mg-Si additive in the fuel (100 X).

Test No. 6 (With 10 ppm V and a Cr-Mg-Si-Additive)

In this test also, the oxide coating showed signs of chipping and spalling after as early as 41 h of exposure to combustion gases. The surface appearance of the NASA- and the Linde-coated specimens after 41 h of exposure is shown in Figures 3-56 and 3-57, respectively. X-ray diffraciton analysis identified predominantly $ZrO_2(Y_2O_3)$ (tetragonal/cubic), SiO_2 (quartz), SiO_2 (cristobalite), $Mg_3(PO_4)_2$ and α-Fe_2O_3 in the surface deposits. Silica is formed by the oxidation of Si in the additive, and $Mg_3(PO_4)_2$ is formed by the reaction of Mg in the additive with P in the combustion gases. Again, no vanadium compound was detected in the surface coating after exposure to combustion gases.

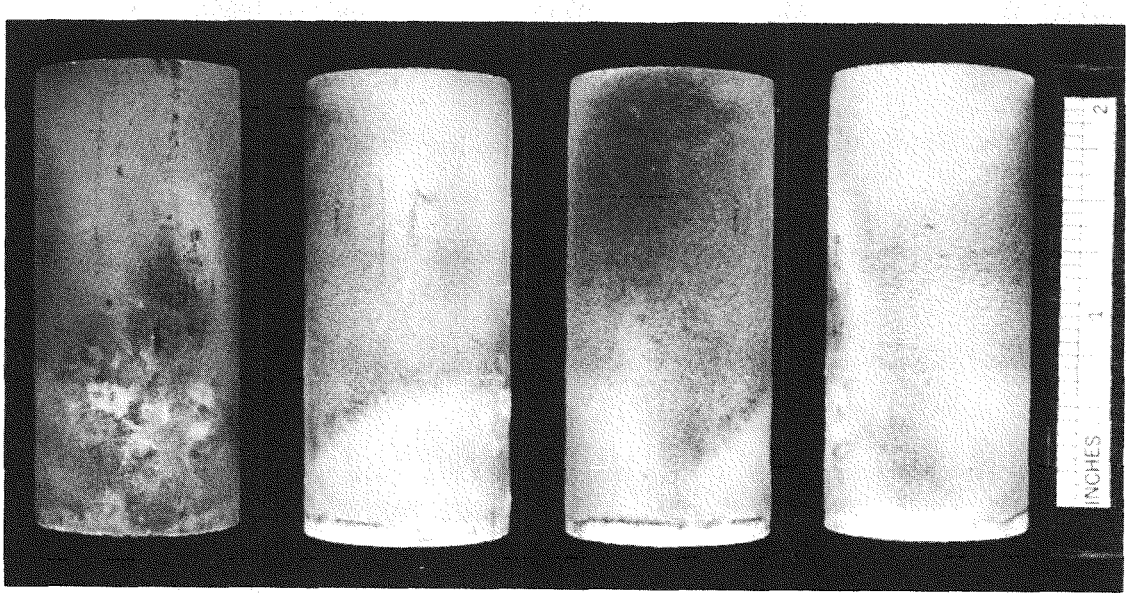

Figure 3-56 Four views of the NASA-coated specimen after 41 h of exposure with 10 ppm V and a Cr-Mg-Si additive in the fuel.

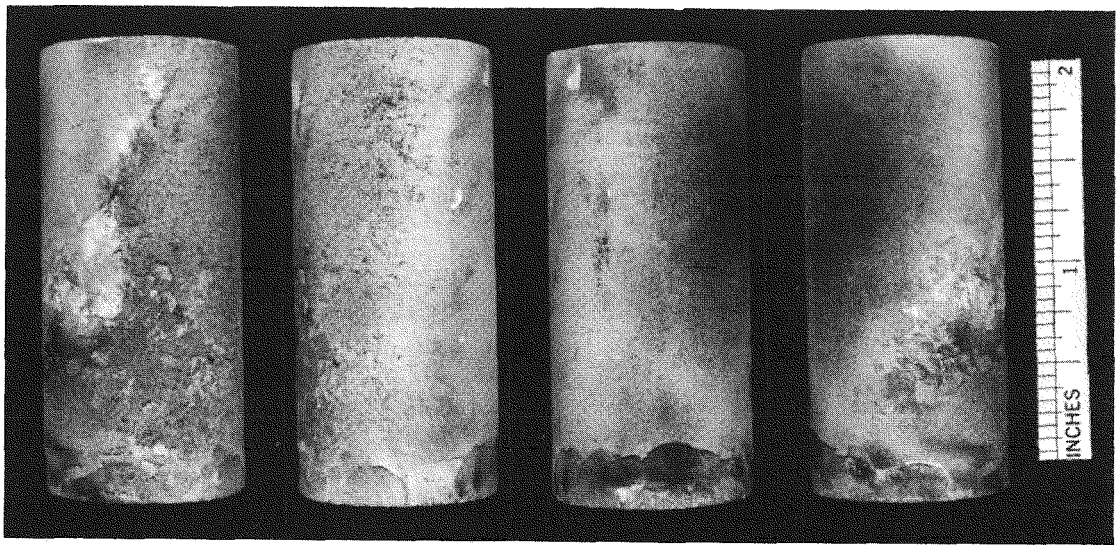

Figure 3-57 Four views of the Linde-coated specimen after 41 h of exposure with 10 ppm V and a Cr-Mg-Si additive in the fuel.

MISCELLANEOUS TESTS WITH MONOLITHIC $ZrO_2(Y_2O_3)$ SPECIMENS

Zirconia stabilized with 12 wt% yttria was plasma-sprayed by NASA-Lewis Research Center in the form of free-standing specimens, 2.0 in. x 0.25 in. x 0.125 in. in diameter. These free-standing bars were used for corrosion and thermal expansion experiments. The purpose of the corrosion experiments was to accelerate possible reactions which could occur in the pressurized turbine passage and better identify the reaction products. The thermal expansion measurements were made to detect any significant densification of the plasma-sprayed $ZrO_2(Y_2O_3)$ on heating to combustion gas temperatures. Volumetric changes due to such densification can give rise to stresses and consequently cracking in the coating. This phase of the program was very cursory in nature due to time limitation. The tests are briefly described below.

Corrosion Tests

Several free-standing $ZrO_2(Y_2O_3)$ bars were coated with Na_2SO_4 and with 1:1 mixture of Na_2SO_4-NaCl in the amounts of 0.5 and 1.0 mg/cm^2. These coated specimens were heated in air at 1800°F for different periods up to 170 h and then analyzed using X-ray diffraction. Only cubic $ZrO_2(Y_2O_3)$ phase was detected in these specimens both before and after the test. All the NaCl and Na_2SO_4 evidently evaporated away during the heating.

Two free-standing ($ZrO_2(Y_2O_3)$ bars were immersed in molten V_2O_5 at 1800°F for a period of 75 h. After the test, visual examination revealed considerable specimen shrinkage which was cuased by liquid phase sintering. X-ray diffraction analysis revealed taht the originally cubic $ZrO_2(Y_2O_3)$ transformed completely in the monoclinic ZrO_2 and, in addition, formed YVO_4. Yttrium oxide in the original cubic phase, thus, reacted with V_2O_5 forming YVO_4 and monoclinic ZrO_2 according to the following reaction:

$$\underset{\text{(cubic)}}{ZrO_2 \cdot Y_2O_3} + V_2O_5 \rightarrow \underset{\text{(monoclinic)}}{ZrO_2} + 2YVO_4$$

This simple test provided important clues to the possible reactions occurring in the pressurized test passage.

Thermal Expansion Measurements

Thermal expansion measurements were made on the plasma-sprayed free-standing $ZrO_2(Y_2O_3)$ bars using a quartz tube dilatometer similar to that described by Valentich (11). The measurements were made in air from room temperature to 2192°F (1200°C) during both heating and cooling cycle. Thermal expansion at various temperatures obtained on the first heating and cooling cycle is shown in Figure 3-58. This data show significant thermal expansion difference between heating and cooling, and also a permanent shrinkage of 0.1%, presumably caused by sintering of the plasma-sprayed $ZrO_2(Y_2O_3)$. Thermal expansion of the same specimen on the second cycle, shown in Figure 3-59, indicated neither significant difference between heating and cooling, nor a permanent dimensional change. Thus, initial heating to high temperatures causes a significant sintering of the plasma-sprayed $ZrO_2(Y_2O_3)$ material.

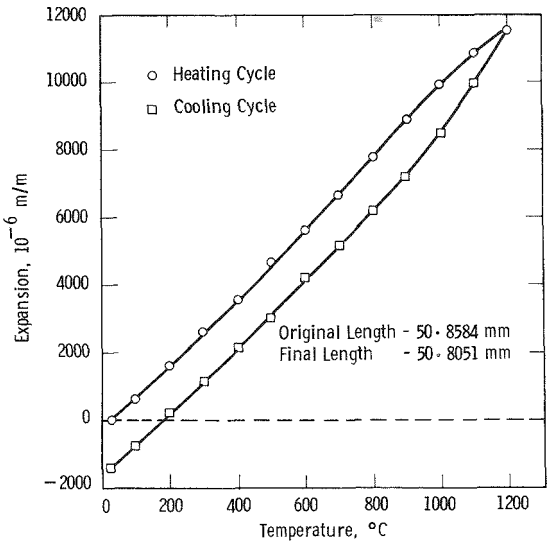

Figure 3-58 Thermal expansion of a free-standing plasma sprayed ZrO_2 (12 wt% Y_2O_3) bar on the first heating and cooling cycle.

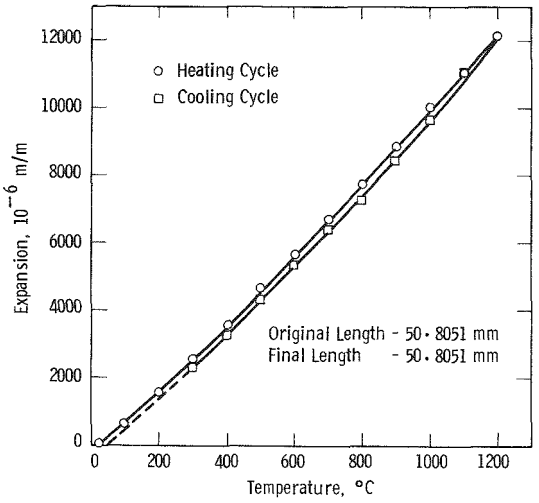

Figure 3-59 Thermal expansion of a free-standing plasma sprayed ZrO_2 (12 wt% Y_2O_3) bar on the second heating and cooling cycle.

Section 4

DISCUSSION

It is evident from the results presented in the previous section that the clean fuel or that containing up to 1 ppm Na or 5 ppm Pb is not detrimental to the ZrO_2 (12 wt% Y_2O_3) coating, at least for the short exposure times of 100-150 h employed in this investigation. However, phosphorous and vanadium in the fuel cause severe cracking and progressive spalling of the oxide coating. Furthermore, coatings from both the NASA-Lewis Research Center and the Linde Division perform similarly under the environments employed in this investigation.

Phosphorous is presented in the clean fuel at a level of 0.3 ppm as shown in Table 1-1. It is also possible that additional phosphorous gets introduced in the combustion gases either through air or through organic additives used to increase the contaminants (particularly sulfur) level in the fuel. The phosphorous oxidizes to P_2O_5 in the combustion chamber and enters the turbine in the gaseous form.* This condensed P_2O_5 (g) apparently reacts with Y_2O_3 in the coating to form YPO_4, and in conjunction with sodium-containing compounds in the combustion gases forms $NaZr_2(PO_4)_3$ according to the following reactions:

$$\underset{\text{(tetragonal/cubic)}}{ZrO_2 \cdot Y_2O_3} + P_2O_5\ (g) \rightarrow 2YPO_4 + \underset{\text{(monoclinic)}}{ZrO_2} \qquad (4\text{-}1)$$

$$\underset{\text{(monoclinic)}}{8ZrO_2} + 4\underline{Na} + O_2 + 6P_2O_5\ (g) \rightarrow 4NaZr_2(PO_4)_3 \qquad (4\text{-}2)$$

$$8ZrO_2 \cdot Y_2O_3 + 4\underline{Na} + O_2 + 14\ P_2O_5\ (g) \rightarrow 4NaZr_2(PO_4)_3 + 16\ YPO_4 \qquad (4\text{-}3)$$

The thermodynamic properties of the reaction products, YPO_4 and $NaZr_2(PO_4)_3$, are not available in the literature and either determined the feasibility and extent of the above reactions, or to estimate the minimum amounts of Na and P in the combustion gases required for the above reactions to proceed. Nonetheless, even though phosphorous is present in the fuel at a low level, it is evident from

*P_2O_5 sublimes at ∿300°C.

the X-ray diffraction and the electron microprobe analysis results that it gets greatly concentrated on the surface of the exposed specimens and forms compounds like YPO_4 and $NaZr_2(PO_4)_3$. Reaction between Y_2O_3 in the coating and P_2O_5 (g) to form YPO_4 leaches out some of Y_2O_3 in the originally cubic/tetragonal $ZrO_2(Y_2O_3)$ solid solution, and thus forms monoclinic ZrO_2 in the oxide coating. This was evident in the X-ray diffraction analysis of the exposed specimens which showed varying amounts of the monoclinic phase. Destabilization of the ZrO_2-Y_2O_3 is a problem as discussed below.

The ZrO_2-Y_2O_3 system has been the subject of many investigations (12-15), but there is no general agreement between the proposed phase diagram. The lower Y_2O_3 limit for the cubic $ZrO_2(Y_2O_3)$ phase field, which is of particular interest in the present study, has been variously determined to be 10 mol % $YO_{1.5}$ by Hund (16), 13 mol % by Duwez, et al. (12), and Srivastava, et al. (13), 15 mol % by Dixon, et al. (17), 16.5 mol % by Schusterius and Padurow (18) and Strickler and Carlson (19) and 14.0 mol % by Forestier, et al. (20). Scott (14) determined this lower limit of cubic solid solution more precisely and showed that it varies significantly with temperature between 1400° and 2000°C. He concluded from this temperature variation that cubic solid solutions in the lower Y_2O_3 range can be prepared at temperatures above 2200° to 1700°C, which if cooled rapidly will be tetragonal at room temperature. The phase diagram of the ZrO_2-rich region proposed by Scott is reproduced in Figure 4-1. It is clear from this diagram that the Y_2O_3 concentrations in the NASA- and the Linde-thermal barrier coatings* actually fall in the two-phase (monoclinic + cubic) field. The fact that the coating consisted of tetragonal/cubic phases even at these lower Y_2O_3 concentrations indicates that the coatings were cooled rapidly from the high temperature used in plasma spraying and thereby quenched in the high-temperature phase. Under these circumstances, appearance of the monoclinic phase in the coatings after extended isothermal exposure to combustion bases is not entirely unexpected. This may explain why the monoclinic phase appeared, although only in trace quantities, even in specimens exposed to clean fuel combustion gases. Furthermore, any reduction in Y_2O_3 concentration, by reaction between Y_2O_3 from the coating and P_2O_5 in the combustion gases, can easily cause formation of the monoclinic phase. This explains the presence of greater amounts of monoclinic ZrO_2 phase in the coating after exposure to the combustion gases with increased contaminants. Monoclinic ZrO_2 phase undergoes phase transformation on heating and cooling with an associated disruptive volume change ($\sim$3 volume percent) leading to cracking and spalling. Formation of other

---

*Linde coating: 11.45 wt% $Y_2O_3 \equiv$ 13.2 mol % $YO_{1.5}$;
NASA coating: 13.30 wt% $Y_2O_3 \equiv$ 15.44 mol % $YO_{1.5}$.

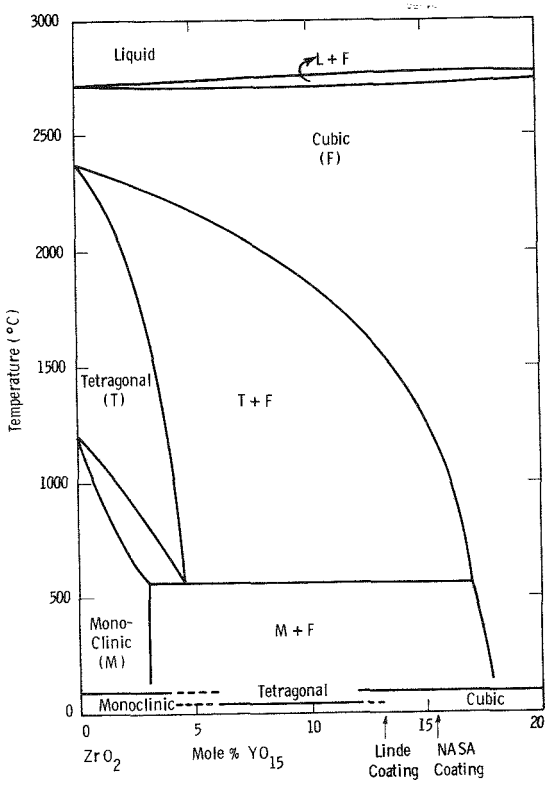

Figure 4-1 Phase diagram for the zirconia-rich region of the ZrO_2-Y_2O_3 system, after Scott (14).

secondary phases such as $NaZr_2(PO_4)_3$ also causes volumetric changes that could lead to cracking and spalling.

Vanadium in the fuel also gets oxidized in V_2O_5 and enters the turbine in the gaseous form. The ZrO_2-V_2O_5 and Y_2O_3-V_2O_5 phase diagrams (21) indicate that V_2O_5 could react with ZrO_2 in the coating to form ZrV_2O_7, and/or with Y_2O_3 to form Y_5VO_{10}, $Y_8V_2O_{17}$ or YVO_4. Contrary to expectations, no vanadium compounds were detected by X-ray diffraction analysis in the oxide coating after exposure to combustion gases even with fuel containing as much as 10 ppm V. Even the reaction between monolithic $ZrO_2(Y_2O_3)$ and molten V_2O_5 formed only YVO_4 (see Section 3). Thus it is apparent that YVO_4 is thermodynamically more stable than any of the other expected compounds. However, even YVO_4 was not detected in the oxide coating after exposure to combustion gases in the pressurized test passage,

even though the electron microprobe analysis indicated that vanadium appreciably penetrated the oxide coating. Vanadium and phosphorous usually form isomorphic (structurally similar) compounds, e.g., YVO_4 and YPO_4; and it is possible that these two compounds formed a solid solution in the exposed oxide coating explainint the absence of YVO_4 lines in the X-ray diffraction patterns. Detailed X-ray diffraction work through use of premixed YVO_4-YPO_4 standards is required to conclusively identify such solid solutions in the coating after exposure to the combustion gases. Also, V_2O_5 is known (22-23) to form glasses with P_2O_5 and many other oxides such as Fe_2O_3, NiO, SiO_2, Na_2O, MgO, etc., which were all present on the surface of the $ZrO_2(Y_2O_3)$ coating after exposure to combustion gases. Thus, V_2O_5 could have easily formed such glasses in the pores of the oxide coating, making their detection by X-ray diffraction impossible. Furthermore, solidification of such glasses from the liquid state in the pores would result in volume shrinkage and the resultant strains could be partly responsible for crack initiation in the coating. In any case, it is apparent that vanadium in the fuel causes severe degradation of the oxide coating through cracking and progressive spalling.

The magnesium-based additives, commonly employed to inhibit the vanadium-corrosion of superalloys and MCrAlY coatings, were found to be ineffective in preventing degradation of the $ZrO_2(Y_2O_3)$ coatings. It appears that elements like P and V are more reactive toward Y_2O_3 in the coating than with magnesium in the additives. Thus, other additives more reactive toward P and V than Y_2O_3 will have to be found if the ZrO_2-12 wt% Y_2O_3 is to be used successfully as a thermal barrier coating. Other appraoches to overcome the detrimental effect of vanadium and phosphorous on the oxide coating have been described (24).

As indicated in Section 3, plasma sprayed $ZrO_2(Y_2O_3)$ undergoes considerable densification (sintering) during heating to ∿2200°F. Such sintering of the oxide coating could also lead to spalling due to reduced thermal shock resistance. This indicates the need for careful preheat treatment of the oxide coating prior to use in order to minimize stresses arising from the volumetric changes due to sintering.

The MCrAlY bond coat was generally not affected in the short exposure times employed in this investigation. However, significant amounts of Na_2SO_4 were found to be present in the coating after exposure to combustion gases containing 5 ppm Na and 0.5 wt% S. This suggests that the bond coat could experience hot corrosion after extended exposure to combustion gases since the oxide coating is porous to start with, and furthermore, gets severely cracked during exposure.

It should also be noted that there is a large difference between the thermal expansion coefficients of the $ZrO_2(Y_2O_3)$ oxide overcoat and the MCrAlY bond coat. The stresses resulting from this thermal expansion mismatch could cause separation of the oxide coating from the MCrAlY bond coat. In the present investigation, in all experiments except for the one carried out with solid pin at 1850°F, there appeared to be no separation of the oxide at the $ZrO_2(Y_2O_3)$/MCrAlY interface, i.e., all cracking and spalling occurred within the thickness of the oxide coating. Thus, under the thermal conditions employed in the present study, chemical reactions rather than thermal expansion mismatch seem to have caused the coating degradation. However, under severe thermal cycling conditions, one should also carefully consider the stresses caused by the thermal expansion mismatch in evaluating the expected performance of duplex thermal barrier coatings.

Section 5

CONCLUSIONS AND RECOMMENDATIONS

1. The ZrO_2·12 wt% Y_2O_3 coating performs satisfactorily in clean fuel and that containing either 1 ppm Na or 5 ppm Pb for 100-150 hr.

2. Vanadium and/or phosphorous in the fuel are detrimental to the ZrO_2·12 wt% Y_2O_3 thermal barrier composition.

3. The principal cause of the failures of the ZrO_2·12 wt% coating is destabilization of the original tetragonal/cubic $ZrO_2(Y_2O_3)$ solid solution.

4. Other possible contributing causes of coating failures are the formation of complex reaction products and localized sintering, both of which contribute to reduced spalling resistance.

5. The duplex thermal barrier concept seems feasible for utility turbine application in that the bond coat alloys (MCrAlY where M = Ni or Ni/Co) protects the base alloy when its temperature does not exceed ∿1650°F.

6. Improved and/or new thermal barrier coatings should be developed specifically for utility turbines burning residual fuels.

7. Rig and engine testing of turbine vanes and blades with thermal barrier coatings should not be conducted until improved coatings are developed and satisfactory laboratory corrosion tests have been obtained for residual fuels.

8. Durability tests should be conducted with clean fuels prior to engine testing.

Section 6

REFERENCES

1. C. H. Liebert and F. S. Stepka. Potential Use of Ceramic Coatings as a Thermal Insulation on Cooled Turbine Hardware. NASA TM X-3352, February 1978.

2. C. H. Liebert and F. S. Stepka. Ceramic Thermal Barrier Coatings for Cooled Turbines. NAS TM X-73426, July 1976.

3. S. R. Levine and J. S. Clark. Thermal Barrier Coatings -- A Near Term High Payoff Technology. NASA TM X-73586, 1977.

4. J. S. Clark, J. J. Nainiger and R. E. Hyland. Potential Benefits of a Ceramic Thermal Barrier Coating on Large Power Generation Gas Turbines. NASA TM 73712, June 1977.

5. R. G. Stabe and C. H. Liebert. Aerodynamic Performance of a Ceramic Coated Core Turbine Vane Tested with Cold Air in a Two-Dimensional Cascade. NASA TM X-3191, January 1975.

6. C. H. Liebert, R. E. Jacobs, S. Stecura and M. C. Robert. Durability of Zirconia Thermal-Barrier Ceramic Coatings on Air-Cooled Turbine Blades in Cyclic Jet Engine Operation. NAS TM X-3410, September 1976.

7. N. Carlson and B. L. Stone. Thermal Barrier Coating on High Temperature Gas Turbine Engines. NASA CR-135147, February 1977.

8. D. J. Amos. Analytical Investigations of Thermal Barrier Coatings on Advanced Power Generation Gas Turbines. NASA CR-135146, March 1977.

9. H. F. Butze and C. H. Libert. Effect of Ceramic Coatings of JT 8D Combustor Liner on Maximum Liner Temperature and Other Combustor Performance Parameters. NASA TM X-73581, December 1976.

10. R. C. Tucker, Jr., T. A. Taylor and M. H. Weatherly. Plasma Deposited MCrAlY Airfoil and Zirconia/MCrAlY Thermal Barrier Coatings. Proc. Third Conference on Gas Turbine Materials in the Marine Environment, University of Bath, England, September 1976.

11. J. Valentich. New Values for Thermal Coefficients. Product Engg. July 19, 1965, p. 63.

12. P. Duwez, F. H. Brown, Jr. and F. Odel. J. Electrochem. Soc., Vol. 98, 1951, p. 356.

13. K. K. Srivastava, R. N. Patil, C. B. Choudhary, K. V. G. K. Gokhale and E. C. Subbarao. Trans. J. Brit. Ceram. Soc., Vol. 73, 1974, p. 85.

14. H. B. Scott, J. Mater. Sci., Vol. 10, 1975, p. 1527.

15. V. S. Stubican, R. C. Hink and S. P. Ray. J. Amer. Ceram. Soc., Vol. 61, 1978, p. 17.

16. F. Hund. Z. Electrochem., Vol. 55, 1951, p. 363.

17. J. M. Dixon, L. D. LaGrange, U. Merten, C. F. Miller and J. T. Porter, II. J. Electrochem. Soc., Vol. 110, 1963, p. 276.

18. C. Schusterius and N. N. Padurow. Ber. Dtsch. Keram. Ges., Vol. 30, 1953, p. 235.

19. D. W. Strickler and W. G. Carlson. J. Amer. Ceram. Soc., Vol. 47, 1964, p. 122.

20. M. Forestier, G. Robert, M. Caillet and C. Deportes. Mat. Res. Bull., Vol. 4, 1969, p. 727.

21. E. M. Levin, C. R. Robbins and H. F. McMurdie. Phase Diagram for Ceramists. Amer. Ceram. Soc. 1969.

22. H. Rawson. Inorganic Glass Forming Systems. Academic Press, New York, 1967.

23. L. A. Grechanik, N. V. Petrovykh and V. G. Karpchenko. Soviet Phys. Solid St., Vol. 2, 1961, p. 1908.

24. R. J. Bratton and S. C. Singhal. Ceramic Thermal Barrier Coatings and Fuel Additives for Electric Utility Gas Turbines Burning Residual Fuels, Westinghouse Disclosure of Invention, RES 78-134, 1978.